


Spring 2018

Imidazolium Ionic Liquids as Multifunctional Solvents, Ligands, and Reducing Agents for Noble Metal Deposition onto Well-Defined Heterostructures and the Effect of Synthetic History on Catalytic Performance

Michael Drake Ballentine

Western Kentucky University, Michael.ballentine128@topper.wku.edu

Follow this and additional works at: <https://digitalcommons.wku.edu/theses>

 Part of the [Environmental Chemistry Commons](#), [Inorganic Chemistry Commons](#), and the [Materials Chemistry Commons](#)

Recommended Citation

Ballentine, Michael Drake, "Imidazolium Ionic Liquids as Multifunctional Solvents, Ligands, and Reducing Agents for Noble Metal Deposition onto Well-Defined Heterostructures and the Effect of Synthetic History on Catalytic Performance" (2018). *Masters Theses & Specialist Projects*. Paper 2101.

<https://digitalcommons.wku.edu/theses/2101>

This Thesis is brought to you for free and open access by TopSCHOLAR®. It has been accepted for inclusion in Masters Theses & Specialist Projects by an authorized administrator of TopSCHOLAR®. For more information, please contact topscholar@wku.edu.

IMIDAZOLIUM IONIC LIQUIDS AS MULTIFUNCTIONAL SOLVENTS,
LIGANDS, AND REDUCING AGENTS FOR NOBLE METAL DEPOSITION
ONTO WELL-DEFINED HETEROSTRUCTURES AND THE EFFECT OF
SYNTHETIC HISTORY ON CATALYTIC PERFORMANCE

A Thesis
Presented to
The Faculty of the Department of Chemistry
Western Kentucky University
Bowling Green, Kentucky

In Partial Fulfillment
Of the Requirements for the Degree
Master of Science

By
Michael Drake Ballentine

May 2018

IMIDAZOLIUM IONIC LIQUIDS AS MULTIFUNCTIONAL SOLVENTS,
LIGANDS, AND REDUCING AGENTS FOR NOBLE METAL DEPOSITION
ONTO WELL-DEFINED HETEROSTRUCTURES AND THE EFFECT OF
SYNTHETIC HISTORY ON CATALYTIC PERFORMANCE


Date Recommended 04-06-18



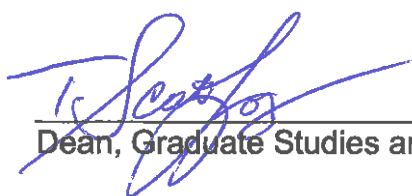
Dr. Lawrence J. Hill, Director of Thesis



Dr. Rui Zhang



Dr. Edwin D. Stevens



Dean, Graduate Studies and Research

4/10/18

Date

ACKNOWLEDGEMENTS

First, this graduate experience wouldn't be possible without Dr. Hill's unbelievable commitment to my education. To look back at my progress over the past two years is just phenomenal. I am at this place in my life because he helped to mold me into the young scientist that I am. He taught me the importance of details and strict discipline. I started as a naïve student who didn't have a path, just a dream. He helped to turn that dream into a reality by pushing me to be my absolute best. He showed me how to be successful and that a good work ethic can take you so much further than natural talent or family status. It is absolutely extraordinary that he had time for anything else judging by the time he put into my education.

I am grateful for the guidance of my research committee, Drs. Stevens and Zhang. I appreciate the time you spent on revising my thesis and listening/challenging my defense.

A special gratitude to Dr. Andersland for many different things. First, he spent 18 hours training me on the TEM and SEM. He also taught me how to carbon-coat TEM grids using two different techniques. I remember one night I was attempting to capture images of a sample and having the absolute worst luck at getting viable images. This goes back to the attention to detail comment I made. Dr. Andersland came in and we were in there until 2am. That kind of dedication is unheard of. We finally left campus with clean images for this thesis.

I would like to thank Pauline Norris at AMI for her guidance. Without her dedication to my work, I would not be able to have much of my data. She spent a

great deal of her time to ensure that I was able to gather the data needed to further my project.

Alicia was a wonderful help throughout my graduate experience. Her knowledge is irreplaceable and much appreciated. Not only that, but her funny stories and patience with a worried and detail-oriented graduate student was really touching. She spent hours and hours on my materials and I cannot thank her enough for her dedication to students.

This thesis wouldn't be complete without a special thanks to Haley Smith. She came in on my orientation day and told us that she was going to be our graduate "momma". I am not exaggerating when I say that I would not be graduating without this woman. She has saved my tail more times than I can count. From making sure that all the proper paperwork is submitted, to helping make sure that I got paid in May of 2017 instead of end of June. I wouldn't have been able to pay rent if she hadn't of been on top of the paperwork. I will miss our talks and will be back to visit!

Other than research, I was a teaching assistant for CHEM 121. I want to thank Dr. Edwards for giving me the support when it came to students. She understood the student dynamic and always addressed concerns with the TA's in mind and that shouldn't go without notice. I also want to thank her for preparing the answer keys and exams for us. I have heard that other TA's are responsible for creating their own exams. That is something that I wasn't required to deal with and I can see the benefit it had with giving me extra time.

I want to also thank the chemistry department for allowing me to pursue my graduate education. They provided me an avenue for success and I simply cannot express how grateful I am. They also provided funding for me to attend the ACS conference in March 2018 along with the Graduate School and the Ogden College.

Last but not least, I want to thank my two best friends that I made at WKU. Mel and Konnor, you two were unbelievable. I have only one thing to say, we made it. Through all the rough times, the organic chemistry, to seminars, to that literature review that almost did us in, we made it. You two will be missed and I couldn't have made it through all this stress without you two. You were truly my rocks to hold on to when I was drowning.

CONTENTS

CHAPTER 1: INTRODUCTION	1
1.1 ELECTRONIC PROPERTIES	1
1.2 SIZE CONTROL	4
1.2.1 <i>Introduction</i>	4
1.2.2 <i>Determining quantum dot diameter</i>	6
1.2.3 <i>Controlling size using ligands</i>	7
1.3 IONIC LIQUIDS	8
1.3.1 <i>Introduction</i>	8
1.3.2 <i>Ionic liquids as a ligand</i>	12
CHAPTER 2: EXPERIMENTAL	14
2.1 MATERIALS	14
2.2 GENERAL PROCEDURES	15
2.2.1 <i>Characterization</i>	15
2.2.1.1 Transmission Electron Microscope	15
2.2.1.2 UV-Vis Spectroscopy	16
2.2.1.3 Fluorometer	16
2.2.1.4 Thermal Gravimetric Analysis	17
2.2.1.5 Inductively Coupled Plasma Analysis	17
2.2.1.6 Karl-Fischer Titration	19
2.2.1.6.1 Working with water standards	19
2.2.1.6.2 Operation of the coulometer 885	20
2.2.1.7 Centrifuge	22

2.2.1.8 Temperature Controller	22
2.2.2 <i>Synthetic Precursors</i>	24
2.2.2.1 CdSe Quantum Dots	24
2.2.2.1.1 Synthesis	24
2.2.2.1.2 Characterization	26
2.2.2.2 CdSe@CdS Nanorods	28
2.2.2.2.1 Synthesis	29
2.2.2.2.2 Characterization	30
2.2.2.3 Thermal deposition: Pt-tipped nanorods	33
2.2.2.3.1 Synthesis	33
2.2.2.3.2 Characterization	35
2.2.2.4 [BMIM]Tf ₂ N	36
2.2.2.4.1 Synthesis	36
2.2.2.4.2 Characterization	38
CHAPTER 3: PLATINUM PHOTODEPOSITION ONTO NANORODS	40
3.1 INTRODUCTION	40
3.2 PHOTODEPOSITION	41
3.2.1 <i>Toluene/TEA</i>	41
3.3 CHARACTERIZATION	47
3.3.1 <i>Cadmium concentration</i>	47
3.3.2 <i>TEM</i>	48
3.4 DISCUSSION	50
CHAPTER 4: PERFORMANCE RESULTS	51

4.1 INTRODUCTION	51
4.2 METHYLENE BLUE DEGRADATION	51
4.2.1 <i>Control Experiments</i>	52
4.2.2 <i>MB degradation in solvent identical to synthesis solvent</i>	53
CHAPTER 5: CONCLUSIONS	59
CHAPTER 6: REFERENCES	62

IMIDAZOLIUM IONIC LIQUIDS AS MULTIFUNCTIONAL SOLVENTS,
LIGANDS, AND REDUCING AGENTS FOR NOBLE METAL DEPOSITION
ONTO WELL-DEFINED HETEROSTRUCTURES AND THE EFFECT OF
SYNTHETIC HISTORY ON CATALYTIC PERFORMANCE

M. Drake Ballentine

May 2018

65 Pages

Directed by: Dr. Lawrence J. Hill, Dr. Rui Zhang, Dr. Edwin D. Stevens

Department of Chemistry

Western Kentucky University

1-butyl-3-methylimidazolium bis(trifluoromethylsulfonyl)imide ([BMIM]Tf₂N) was investigated as a multifunctional solvent, ligand, and reducing agent for platinum deposition onto well-defined CdSe@CdS nanorods. Platinum deposition was carried out thermally and photochemically using Pt(acac)₂ as the metal precursor. Thermal deposition was investigated in [BMIM]Tf₂N with and without addition of a sacrificial reducing agent, and product topology was compared with the products obtained from polyol reduction using 1,2-hexadecanediol, oleic acid, and oleylamine in diphenyl ether. Photochemically induced platinum deposition was carried out at room temperature in [BMIM]Tf₂N, and product topology was compared with the photodeposition products obtained from a toluene dispersion. Thermal deposition of platinum in ionic liquid showed rods of broken morphology and small platinum nanoparticles speckled across the rods' surface, while photodeposition of platinum exhibited particles decorated throughout the nanorod surface but larger in size than those exhibited by thermal means. Photocatalytic

reduction of methylene blue was studied using these Pt-CdSe@CdS heterostructured nanoparticles, and catalytic performance was correlated with topology and synthetic history. Initial findings of catalytic performance suggest that there is an advantage of depositing platinum nanoparticles onto the CdSe@CdS in the ionic liquid system. Methylene blue dye was degraded using each system and the results show an increased performance of the nanorods synthesized in the ionic system.

Chapter 1: INTRODUCTION

1.1 Electronic properties

The optoelectronic properties of semiconductor nanoparticles strongly depend on size giving the opportunity for tunability. The ability to control the size of band gaps is one of the key reasons why these particles are commonly synthesized. The band gap of cadmium sulfide (CdS) in particular can be tuned between 4.5 and 2.5eV as cluster size is varied.¹⁻² Figure 1.1 compares electron transitions of semiconductors and metals. Because the Fermi level (level at which no electrons have enough energy to ascend to a higher molecular orbital without an outside influence) of a semiconductor is in-between the energy states of the material, the optical and electronic properties strongly depend on the size of the particle. As the particle size increases, the energy bands become closer together. This gives a control over energy band positioning which enables applications such as electron confinement and an array of color emission.

The catalytic activity of particles is strongly correlated to their size.² Figure 1.2 illustrates gold nanoparticles supported on titania.³ As the size of the particle decreases, the surface area to volume ratio increases and exponentially increases the total catalytic activity. This effect illustrates the importance of tuning the particle size to achieve the highest catalytic activity and maximum reactivity.²⁻³ There is a decrease in activity observed once the particles size decreases below 3.5 nm (diameter) and 1.0 nm (height). This is caused by a metal-to-nonmetal transition.

The size at which this transition occurs will depend on the composition of the nanoparticles.²

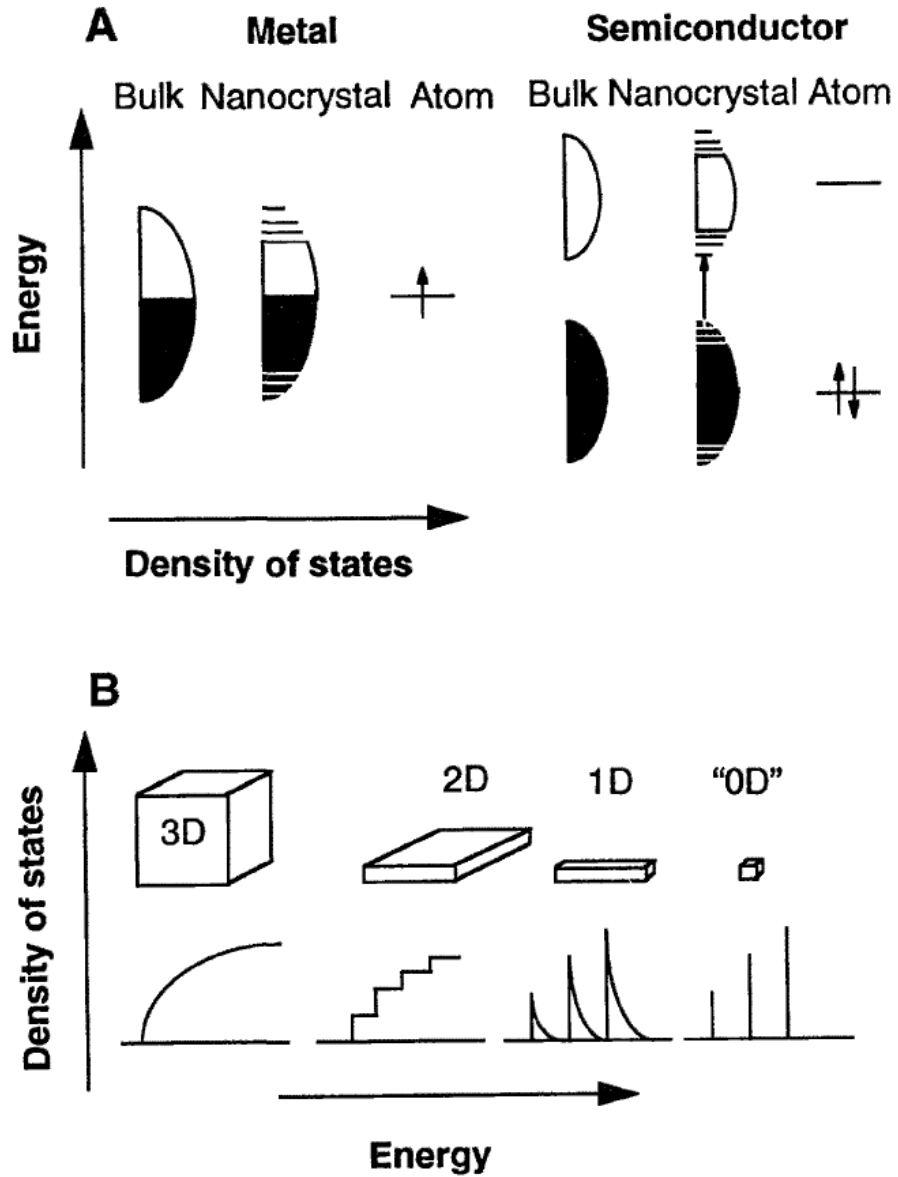


Figure 1.1. Difference in electronic structure of a metal and a semiconductor. (A) Illustration depicting the density states of metals and semiconductors. (B) Dimensional representation of a single band of a semiconductor. (Copyright from ref. 1).

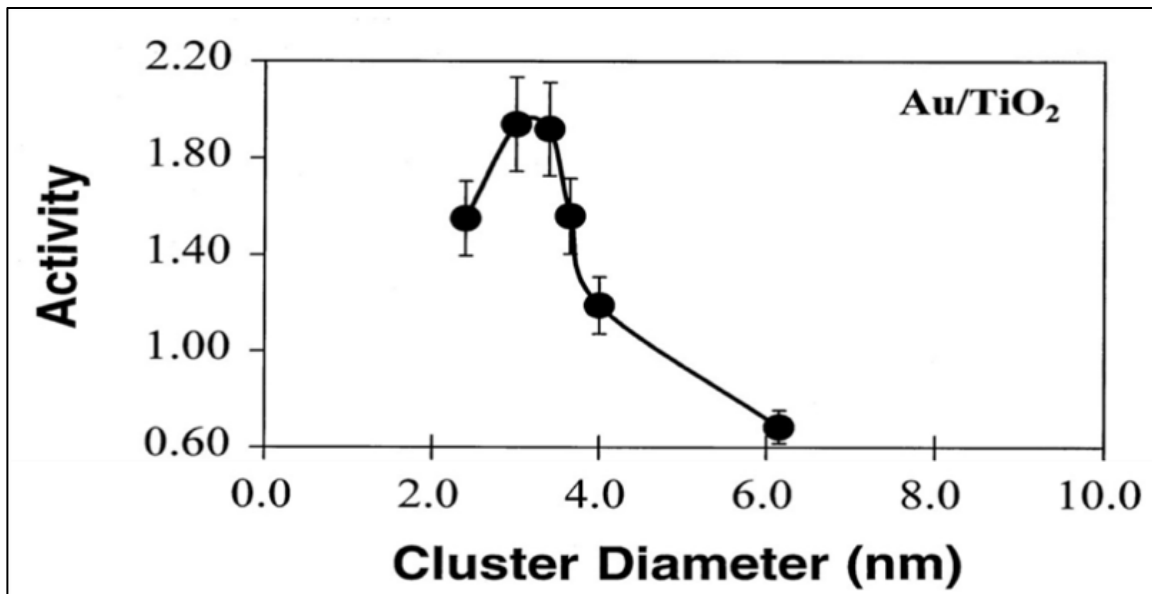


Figure 1.2. Correlation between particle size and activity for TiO₂-supported Au nanoparticles. As size is decreased, the surface area to volume ratio is exponentially increased. This allows for a maximum output of activity. The decrease in activity for particles smaller than 3.5 nm is caused by a metal-to-nonmetal transition for this material. (Adapted from ref. 2)

Figure 1.3 shows two situations for a heterojunction between CdSe, CdS, and Pt. In situation A, both the valence band and conduction band of CdSe are slightly higher than those in CdS (a type II junction). Thus, any electrons excited in CdS have the possibility of relaxing to Pt, but not CdSe. In situation B, the conduction band gap of CdSe is lower than that of CdS, and any electrons excited in CdS may relax to either Pt or CdSe (type I junction). This figure shows an example where controlling the size of CdSe could be used to change its bandgap and achieve the desired charge transport properties (a type I or type II junction).

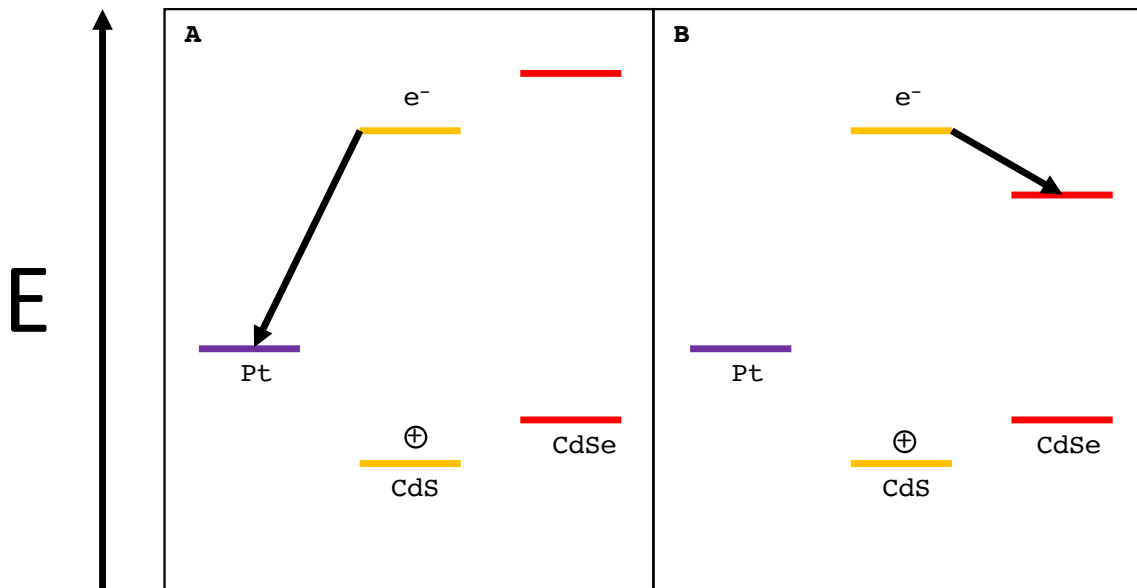


Figure 1.3. Band gap diagram depicting heterojunctions containing smaller (A) and larger (B) cadmium selenide (CdSe) particles.

1.2 Size Control

1.2.1 Introduction

Figure 1.4A illustrates the correlation between the growth rate and radius/critical radius (r/r^*) of nanoparticles. When the radius (r) of nucleated particles exceeds the critical radius (r^*), growth will occur. Figure 1.4B illustrates LaMer's classic stages of particle growth.⁴ When a monomer is introduced into a reaction mixture, the critical concentration (C_{\min}) is achieved and nucleation occurs (stage 1) until the monomer saturation decreases below C_{\min} and nucleation stops (stage 2). This causes a decrease in monomer concentration allowing for particle

growth to continue (stage 3). As the concentration of monomer approaches the lower saturation limit (C_s), smaller particles will begin to dissolve due to a negative growth rate causing larger particles to grow at a faster rate. This phenomenon is known as Ostwald ripening and may be counteracted by the introduction of additional monomer.⁵

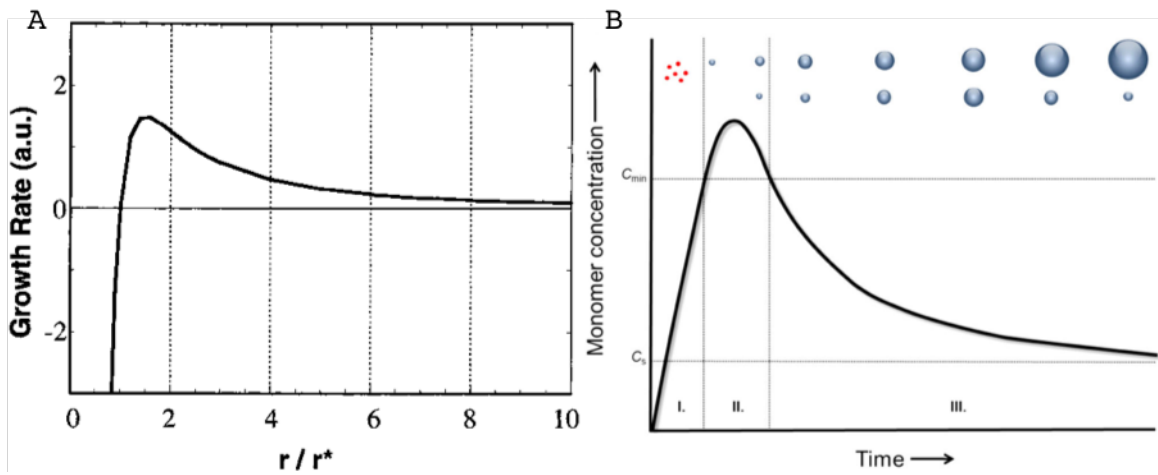


Figure 1.4. (A) Correlation between growth rate and the critical radius (r^*) for which the solubility of the nanoparticle is exactly the concentration of the monomer in solution (zero growth rate). (B) Classic LaMer model showing three stages of particle growth: (I) introduction of monomer allowing the critical concentration (C_{min}) required for nucleation to be reached; (II) nucleation partially relieves the monomer saturation; (III) monomer concentration drops below the requirement for nucleation and particle growth occurs until monomer is depleted and the reaction approaches the lower solubility limit (C_s). (Figure adapted from ref. 4-6).

1.2.2 Determining quantum dot diameter

There is a strong correlation between the diameter of quantum dots and the first absorbance peak of their UV-Vis absorption spectra.⁶ Figure 1.5 illustrates absorption spectrum corresponding with three lab-synthesized samples of cadmium selenide (CdSe) quantum dots. Equation 1 is an empirical fit discovered by Peng and coworkers which helps to determine the average particle size of a CdSe quantum dot sample by inputting the maximum absorbance value of the first UV absorption peak (λ).⁶

$$(1) D = (1.6122 \times 10^{-9})\lambda^4 - (2.6575 \times 10^{-6})\lambda^3 + (1.6242 \times 10^{-3})\lambda^2 - (0.4277)\lambda + 41.57$$

As average particle size changes, smaller particles will exhibit an observable blue-shift in UV absorption because of a larger band gap.^{1, 7} The larger band gap will require a photon with a shorter wavelength for electron excitation because wavelength is inversely proportional to energy.

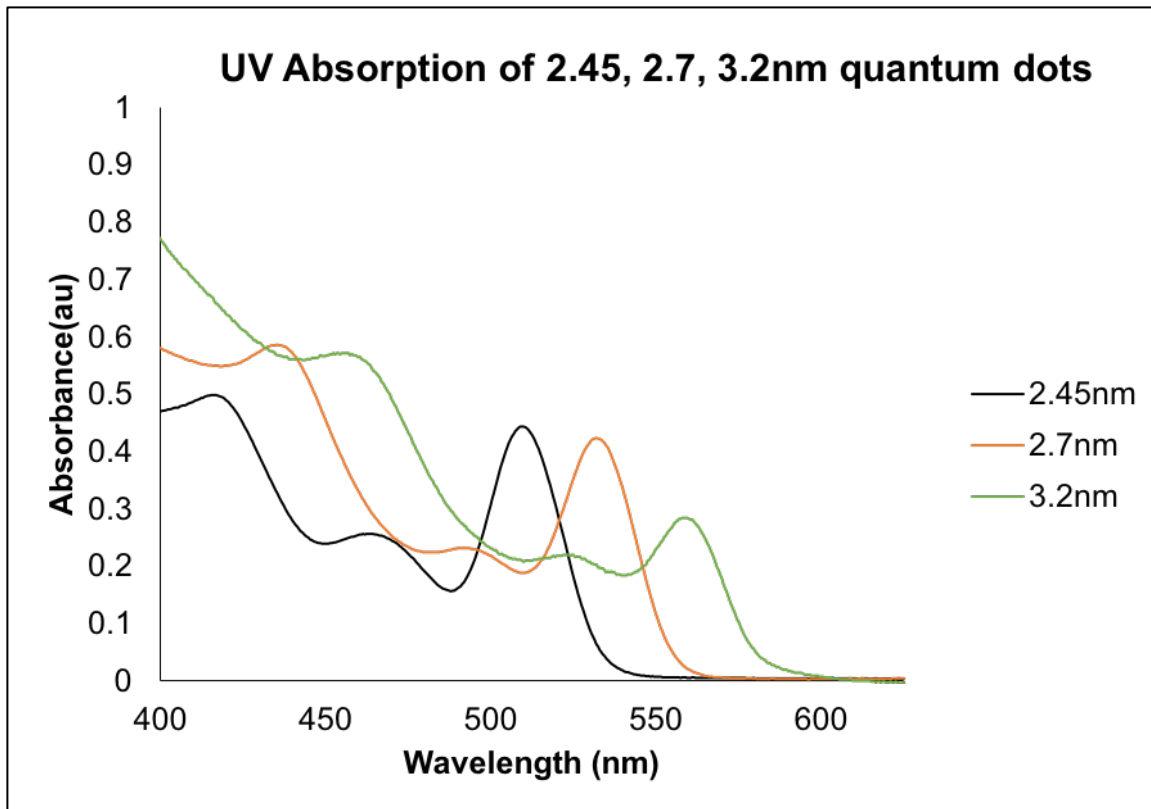


Figure 1.5. Absorption spectra of three lab synthesized quantum dots with peaks at 510 (d = 2.5 nm), 532 (d = 2.7 nm), and 559 nm (d = 3.2 nm).

1.2.3 Controlling size using ligands

The use of strongly binding ligands to control the size and shape of nanoparticles gives distinct advantages over varying the concentration of monomers. The desired growth rate can be achieved by using certain surfactants to prevent ripening from occurring.⁸ The ability to control the size of particles has led to studies of quantum confinement and can yield samples with the desired optical properties, but there is a disadvantage of using these strongly binding ligands. Even though they give incredible control over the particles' size and

shape, they decrease their catalytic activity by decreasing the available surface area. New research into using ionic liquids as a weakly binding ligand has provided an alternative to the classic strongly binding ligands.⁹

1.3 Ionic Liquids

1.3.1 Introduction

Ionic liquids (ILs) are salts that are liquid below 100°C because of the bulky nature of their ions which causes a poor packing efficiency allowing for the free movement of ions.¹⁰⁻¹¹ Generally, the more bulky the ions, the lower the melting point will be. Chart 1.1 illustrates the IL, 1-butyl-3-methylimidazolium bis(trifluoromethanesulfonyl)imide ([BMIM]Tf₂N). It has a melting point of -4°C and begins to decompose at around 280°C. The properties of ILs change depending on what ions make up the compound. For this reason, ILs are known as designer solvents because a selected combination of cation and anion can be made to get the desired properties.

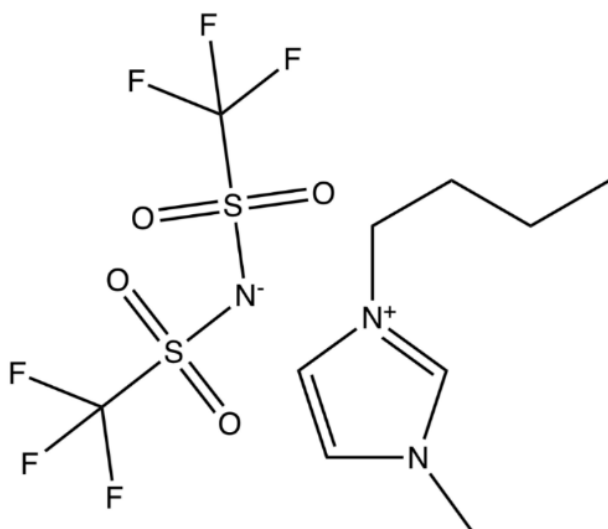


Chart 1.1. 1-butyl-3-methylimidazolium bis (trifluoromethanesulfonyl)imide ([BMIM]Tf₂N). The compound contains both a bulky cation and anion. It has a melting point of -4°C and a onset degradation temperature around 280°C.

The thermal stability of ionic liquids depends strongly on the ions.¹² For example, dialkylammonium containing ILs begin to decompose at around 80°C while [BMIM] containing ILs typically start around 250-350°C depending on the anion.¹³ Figure 1.6 illustrates thermal analysis of [BMIM]Tf₂N indicating that a weight change begins to occur at around 350°C.¹¹ The high thermal stability of ILs along with their ability to provide a polar, weakly coordinating medium can have benefits in nanoparticle synthesis that other organic solvents cannot offer. Figure 1.7 gives a list of various ionic liquids and their corresponding decomposition onset temperatures.¹⁴

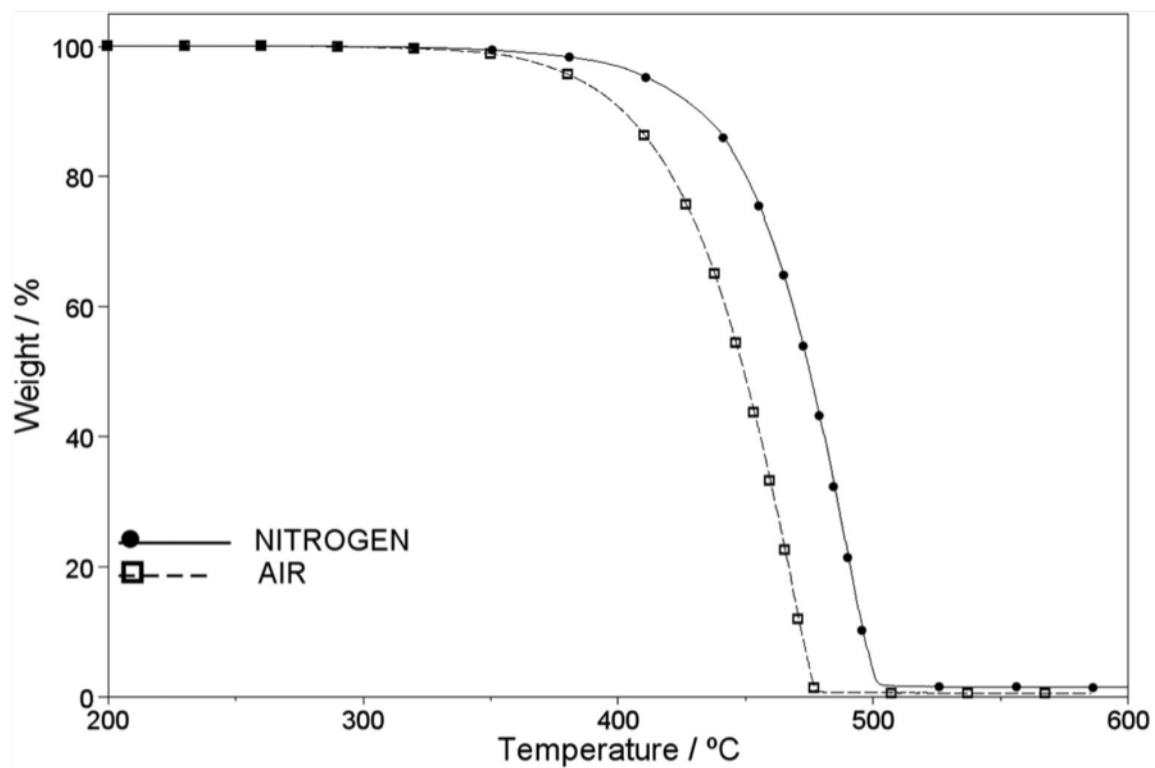


Figure 1.6. Thermal analysis of [BMIM]Tf₂N in an air and nitrogen atmosphere. TGA data illustrates the change in weight percent of sample as a function of temperature. (Figure adapted from ref. 9).

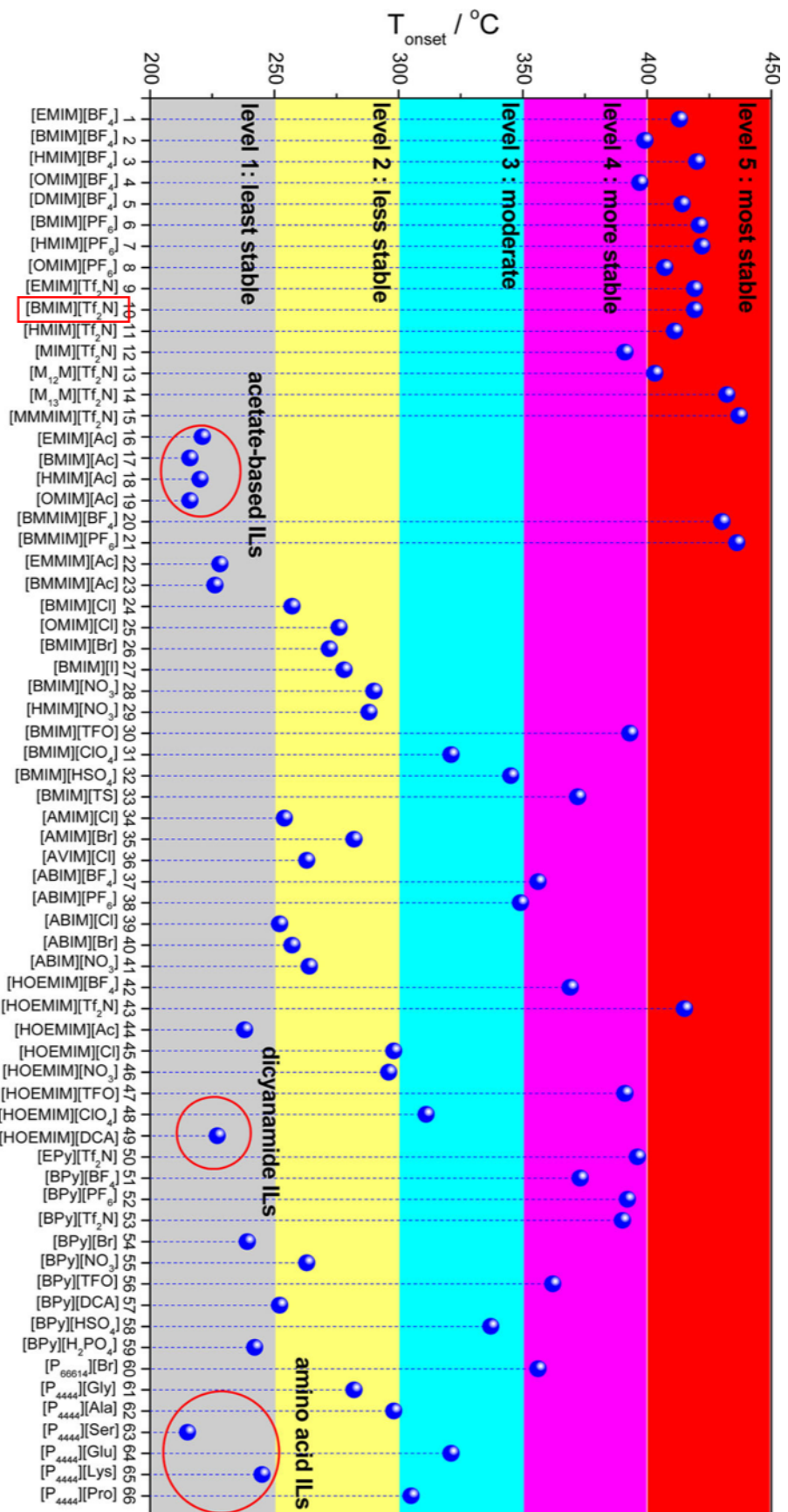
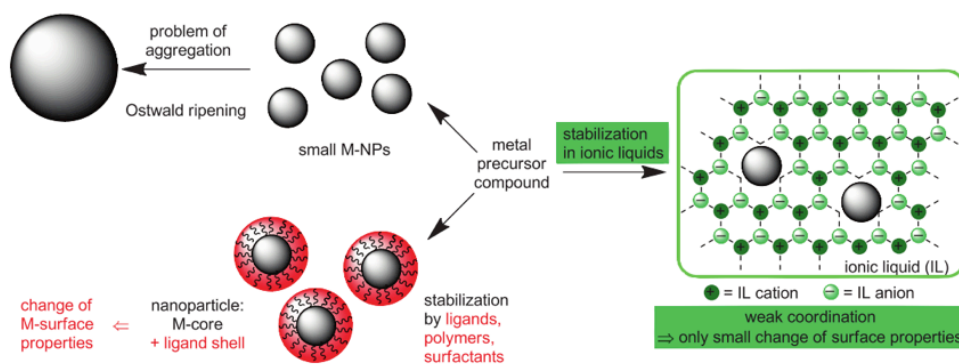


Figure 1.7. List of the decomposition onset temperatures for different ionic liquids. [BMIM][Tf₂N] is indicated with a red box. (Adapted from ref. 12).

1.3.2 Ionic liquids as a ligand

Scheme 1.1 illustrates a comparison between using an ionic liquid and using a traditional ligand to stabilize nanoparticles.¹⁵ A supramolecular ionic liquid network stabilizes metal nanoparticles through electrostatic and steric forces by the formation of an ion layer around the particles. ILs containing both the [BMIM] cation and a relatively weakly coordinating anion such as BF_4^- , PF_6^- , or Tf_2N^- will allow for a physicochemical phenomenon known as the IL effect: a spontaneous, well-defined structural organization of the ionic liquid matrix.¹⁶⁻¹⁸ This IL effect will allow for the stabilization of small particles without decreasing the available surface area.



Scheme 1.1. Three scenarios for the stabilization of metal nanoparticles. (Green) Metal nanoparticles are supported by the supramolecular ionic liquid network through electrostatic and steric stabilization. (Red) metal nanoparticles are stabilized through electrostatic and steric stabilization. (Red) metal nanoparticles are stabilized using traditional tightly binding ligands. (Gray) Metal nanoparticles are not stabilized with additional surfactants resulting in aggregation. (Copyright from ref. 14).

The purpose of this research is to implement the ionic liquids to gain control over the shape/size of heterostructured nanoparticles while maintaining the surface availability needed for efficient catalysis. This approach will provide the benefits of control that the tightly binding ligands provide without the drawbacks. The IL loosely binds to the surface of the particle preventing aggregation and then will “let go” allowing the particle to move freely throughout the complex matrix of the liquid without it coming in contact with another particle.

Chapter 2: EXPERIMENTAL

2.1 Materials

Most solvents used were purchased from Sigma Aldrich Chemical Company without any additional purification. These solvents include acetone, chloroform, dichloromethane (DCM), ethanol, hexane, methanol, and toluene. Cadmium oxide (CdO) was purchased from both Sigma Aldrich and Strem, inc. It was found that the CdO purchased from Strem had unoxidized cadmium within the reagent resulting in unexpected black precipitate material in the quantum dot products. This caused a change of reagent to Sigma Aldrich after which all black precipitate did not reappear. Platinum (II) acetylacetonate, selenium powder, sulfur, trioctylphosphine oxide (TOPO), trioctylphosphine, n-octadecylphosphonic acid (ODPA), 1,2-hexadecanediol (HDD), hexylphosphonic acid (HPA), lithium bis(trifluoromethylsulfonyl)imide salt, and [BMIM]Cl were purchased from Sigma Aldrich. The selenium powder was further purified of any water by drying at 240°C for 24 hours in a vacuum oven.

2.2 General Procedures

2.2.1 Characterization

2.2.1.1 Transmission Electron Microscope

Samples were imaged using a JEOL 1400Plus transmission electron microscope using both the 100kV and 120kV voltages. Copper 200 mesh grids with a carbon coating were used as a sample holder to get the images. The grids used to image the particles were coated in lab. The fixtures which hold the carbon are from Ladd Research Industries: 30170 - Carbon Rod Evaporation Unit 30180 - Carbon Evaporation Shield. The carbon was from EMS Cat #70200, sharpened to about 4 mm with a #12040 carbon rod sharpener from E. Fullam. The glass shield was coated with "Bell Shine" from Ladd #30099. Any vacuum evaporator can be used with the Ladd fixtures. Our Vacuum Evaporator was built by Torr International, Model number: TH#-2KW-UPGRD-EB1P operated initially in the 10-6 torr range vacuum range, and at about 40 Amps. The mica was fixed into a clean petri dish which was then placed on a 50 mL beaker making it approximately 5-10cm from the graphite rod. The mica was coated using an indirect coating method using a quarter affixed directly above the mica so that the coating would be a consistent thickness and to reduce the overall thickness of the coat.

The mica was cut into small squares (approximately the size of a grid) and gently placed on a droplet of water. Because mica is hydrophilic and carbon is

hydrophobic, the mica sank to the bottom of the water leaving a thin film of carbon floating on the water droplet. That allowed for a copper grid to be carefully placed into the water droplet and under the carbon film. The grid was then lifted so that the carbon film was coated onto the surface of the grid was then placed on filter paper to dry.

2.2.1.2 UV-Vis Spectroscopy

UV-Vis spectroscopy was performed using a UV-2600 UV-VIS Spectrophotometer by Shimadzu. A 0.5 mL quartz cuvette was used as a sample container. An empty cuvette was used as a blank and was subtracted out of the spectra. The instrument method was set to scan from 700 nm to 300 nm with 0.5 nm increments and “medium” method. It was found that higher than medium provided spectra of “choppy” data. The data was then saved as “data print table” (.txt file) that Microsoft Excel then imported and allowed for analysis. If the file was saved as the default file selection, only the software provided by the manufacturer was able to open it.

2.2.1.3 Fluorometer

The fluorometer used was a Shimadzu RF-5301 PC spectrofluorometric. The samples were diluted in a 5 mL quartz cuvette using the solvent native to the system being tested. An empty cuvette was used as a blank and was subtracted

out of the spectra. The instrument was set to a medium scan rate to balance both time and quality data. It was noted that if the instrument was set to anything slower, it would take around an hour per sample with minimal effect of spectral quality. The raw data were saved and analyzed using Microsoft Excel.

2.2.1.4 Thermal Gravimetric Analysis

Thermal analysis was performed using a Netzsch STA Jupiter STA449F1 TGA-DSC. The program used was a 10°C/min ramp rate with a 10-minute hold at 100°C to ensure all water was extracted from the system. The instrument would then ramp to 600°C and complete the test. This data was extracted as a text file and analyzed using Microsoft Excel.

2.2.1.5 Inductively Coupled Plasma Analysis

In order to determine the cadmium concentration in the Pt-tipped nanorod (Pt-NR) samples, a ThermoScientific ICAP 6500 ICP-OES was used. A series of standards were prepared using standards purchased from Inorganic Ventures (Lot F2 – CD02035 3% Nitric acid, 1000µg/ mL) and nanopure water to the appropriate concentration. Concentrated HCl (25 mL) (tracemetal grade, Fisher Scientific UN1789) was added to the standards. These solutions were then diluted up to 50 mL with nanopure water. For these particular experiments, different standards were created. It was determined after two trials, that the standards were best

between the concentrations of 0.01-1 mg/ mL. This was the range of the cadmium and sulfur concentrations. The increments of standards are not important as any standards within this range will provide accurate results. Also to note, there is no need to prepare completely new standards for each of the type of element being tested. For instance, the sulfur and cadmium standards were included in the exact same ICP bottles. Pt(acac)₂ was used as a platinum standard after the first trials and therefore did not contain cadmium and sulfur in the standard solutions. There was also a blank that was prepared with nanopure water (25 mL) and concentrated HCl (25 mL).

The Pt-NR's synthesized in both toluene and [BMIM]Tf₂N were analyzed in the following way. Purified Pt-NRs product (0.05 mL) was placed in a 50 mL ICP container and allowed to evaporate (the product was stored in toluene). This took around 5 minutes. Once the toluene had evaporated and there was no visible solvent remaining, concentrated HCl (10 mL) was added to dissolve the dried product with slight mixing. Nanopure water (25 mL) was then added to dilute the acid and then the bottle was filled using concentrated HCl (15 mL) to a total volume of 50 mL of solution.

The ICP was programmed and given a name of "Drake's Method" for future experiments. This method included the standard concentrations, sample numbers/names, and wash time (8 seconds). It was found that if wash time was shorter, that contamination and inaccuracy could arise. Also, it is important to place two blanks between the standards and the experimental samples to ensure the

system is completely washed of the standard solutions before the introduction of an unknown sample.

2.2.1.6 Karl-Fischer Titration

2.2.1.6.1 Working with water standards

The 1.0 mg/g water standard was easier to handle and was therefore preferred. If a 0.1 mg/g water standard is used, then a glass syringe must be used but if a 1.0 mg/g water standard is used, then a plastic syringe may be used. Using a clean syringe, a new ampoule of water standard was taken and shook briefly to ensure homogenous contents. With a folded paper towel held between thumb and index finger, break open the ampoule at the marking and draw up water standard (1 mL) into the syringe. Pull the plunger of the syringe up to the end and shake the syringe back and forth. The inside of the syringe is rinsed by water standard and freed of any water contamination. Dispose of that used water standard into a waste bottle. Draw the rest of the water standard into the syringe, aspirating as little air as possible. Push out any air bubbles that may be present in the syringe and wipe off the needle with a lint-free paper towel. Place the syringe on the balance and tare. As soon as the drift on the 899 Coulometer is stable, take the syringe in your hand, press start on the instrument, and inject 1 mL of water standard through the septum. Close the syringe with the same cap and place it back on the balance.

Read off the value displayed by the balance and enter it on the coulometer as the sample size.

2.2.1.6.2 Operation of the coulometer 885

Start Sequence - This command sequence is run one time after the method has been started. It is used for conditioning the entire system. The oven is heated to the set temperature. The tubing system is flushed with the carrier gas until all moisture has been expelled. The moisture is titrated in the titration cell. The titrator is connected with the 885 Compact Oven SC using a remote cable. The instrument starts conditioning at the titrator through the remote cable control line. Once the titration cell is conditioned, the titrator switches a signal line to active. This signal line is monitored by the 885 Compact Oven SC. Move to the conditioning beaker, lower lift, pierce vial, switch on the gas flow, start conditioning at the titrator, heat the oven to the configured temperature, and wait until conditioning is complete. The signal line **Cond OK** must be active for 60 s.

Sample Sequence – This command sequence is executed for every sample (or blank). It is repeated for each sample. The total number of samples (or repetitions) and the rack position of the first sample (or blank) are entered when the method is started. Scan the **Cond OK** signal of the titrator, start the titration at the titrator, switch off the gas flow, move to the sample vial, lower lift, pierce vial, move vial into oven, switch on the gas flow, record temperature and gas flow, wait for end of titration (EOD signal), copy report to USB, switch off the gas flow, move

to the conditioning vial, lower lift, pierce vial, switch on the gas flow, wait until condition is complete, the signal line **Cond OK** must be active for 60s

End Sequence – This command sequence is run one time after the last sample sequence. The parameter End of series can be used to control a slightly variant behavior. Switch off the gas flow, move to the conditioning beaker, **do not lower the lift**, stop titrator (**only with End of series = Stop**) (the titrator is not stopped with End of series = Conditioning, i.e. the titration cell continues to be conditioned), and switch off the oven heating.

Sample Water Content (%)	Coulometric Sample Size (g)
100	Not Recommended
50	≤0.01
10	0.01 - 0.05
5	0.05 - 0.10
1	0.10 – 0.2
0.5 (5000 ppm)	0.20 – 1.00
0.1 (1000 ppm)	1.00 – 2.00
0.01 (100 ppm)	2.00 – 5.00
0.001 (10 ppm)	5.00 – 10.0
0.0001 (1 ppm)	≥10.0

Table 2.1. Comparison between expected sample water content and the approximate weight of your sample. This will ensure that both time and accuracy are maintained.

2.2.1.7 Centrifuge

The centrifuge used for the purifications was a Thermo Scientific Sorvall ST 8 having a radius of 0.12 m. Standard 50 mL centrifuge tubes were used for the synthesis reactions. It was found that the maximum spin rate for these tubes and this centrifuge was 7000 rpm. Any higher spin rate was found to crack/break the tubes.

2.2.1.8 Temperature Controller

During thermal reactions, a constant and consistent temperature is a very crucial part. It was noticed that the temperature fluctuation delivered by the temperature controller was varying out of the expected range. Figure 2.1 shows a set of experiments that were conducted to measure the change in temperature as a function of time. The temperature controller has two different connections to allow it to output two different temperature programs. The controller was programmed to output a 240°C reaction vessel temperature. Temperature output 1 had the highest variation in temperature of $\pm 80^{\circ}\text{C}$. This is too much variation in temperature for the temperature sensitive nanoparticle syntheses. Output 2 showed a slight improvement in variation of $\pm 40^{\circ}\text{C}$ but was still not acceptable. Note that output 1 and 2 do not affect each other. They have their own programming. Using the auto calibration input function of the temperature

controller, the temperature output 1 was refined to a more reasonable $\pm 1^\circ\text{C}$. The initial dip in temperature seen around 10 minutes was the instrument adjusting to the reaction environment temperature and automatically adjusting how much energy is was outputting in order to achieve the 240°C target. By these results, it is recommended to allow at least 20 minutes for auto adjustment completion before beginning a reaction.

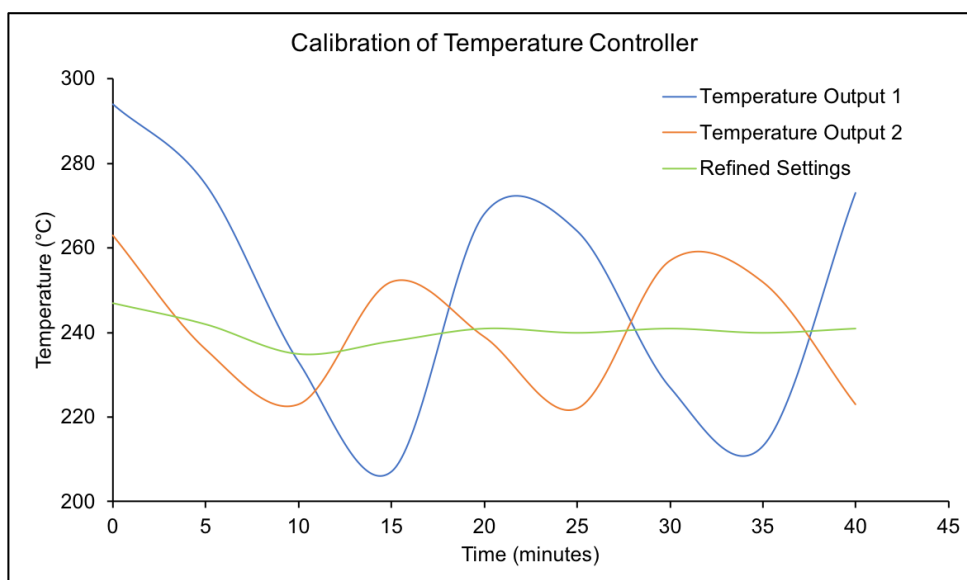


Figure 2.1. Calibration of thermal temperature controller. The temperature controller had two separate outputs that could control the temperature of a reaction mixture. Temperature output 1 varied the most with a $\pm 80^\circ\text{C}$ while output 2 did not vary quite as much with a $\pm 40^\circ\text{C}$. Once the settings had been calibrated and refined, the variation was reduced to a more acceptable $\pm 1^\circ\text{C}$. The initial dip at 10 minutes was the instrument automatically adjusting the amount of heat that was delivered to the reaction vessel. Note that the target temperature for all these trials was 240°C , a typical temperature for a nanoparticle synthesis.

2.2.2 Synthetic Precursors

2.2.2.1 CdSe Quantum Dots

2.2.2.1.1 Synthesis

Figure 2.2 illustrates the synthesis of cadmium selenide quantum dots as adapted from literature.^{1, 19}

Elemental selenium (1.4g) was added to a 20 mL vial, sealed, and evacuated of air and backfilled with an inert gas. Trioctylphosphine (TOP) (10 mL) is then added to the vial. The mixture was stirred overnight at 300 rpm.

CdO (0.18g), ODPA (0.84g), and TOPO (9g) was loaded in a clean 100 mL three-neck round-bottom flask with a 1-inch stir bar. The mixture was heated to 150°C for 30 minutes under vacuum with stirring at 300 rpm. The vessel was then backfilled with argon and heated to 300°C. Once the solids were fully dissolved and the solution became clear, TOP (5.5 mL) was added. The solution was then heated to 380°C. The stock solution (1.2 mL) of TOP:Se was quickly injected and the solution was allowed to react for 6-15 seconds depending on the desired size of the dots. ODE (15 mL) was then injected over 10 seconds to quench growth. Toluene (20 mL) is added at 110°C to prevent solidification.

Crude product was divided evenly between 2 centrifuge tubes and diluted with toluene (up to a total volume of 25 mL) and precipitated with ethanol (25 mL).

Tubes were then centrifuged for 7 minutes at 7000 rpm. Supernatant was decanted and the pellet was dispersed in toluene (20 mL). These steps were then repeated 2 more times. The product (pellet) was then transferred into a tared vial and dispersed in DCM and dried with a rotovap.

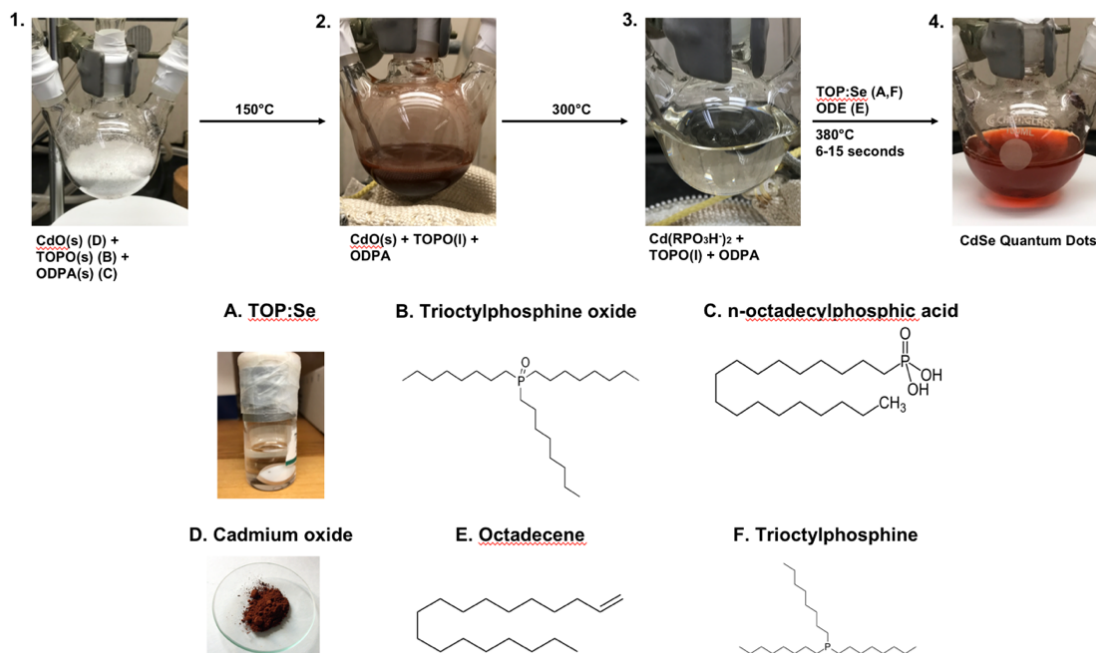


Figure 2.2. CdSe quantum dot synthesis. (1) Cadmium oxide (D), trioctylphosphine oxide (B), and octadecylphosphonic acid (C) are heated to 150°C. (2) Opaque mixture is heated to 300°C under inert gas creating a cadmium phosphonate complex. (3) Clear solution (cadmium phosphonate complex) is heated to 380°C and a stock solution (A) (trioctylphosphine (F) and elemental selenium) is injected. 1-octadecene (E) is injected slowly over a 10 second period.

2.2.2.1.2 Characterization

Figure 2.3 also shows the fluorescence emission spectra of the 2.45 nm quantum dots. The sample was excited by a 350 nm excitation wavelength which caused the peak at 700 nm (not depicted in figure). The fluorescence emission was measured as a function of wavelength and is red-shifted from the absorption peak.

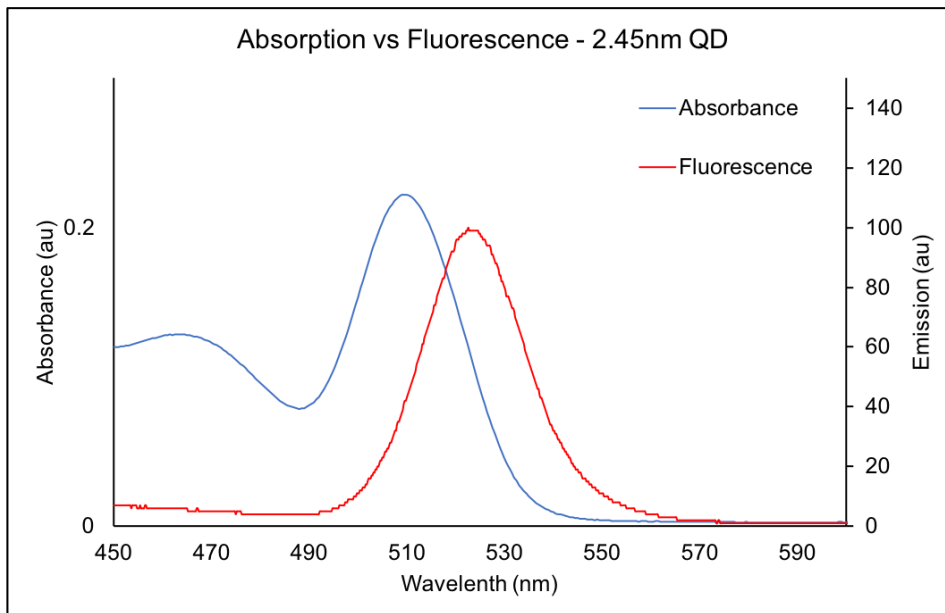


Figure 2.3. Absorption and emission spectra of 2.45 nm CdSe quantum dots. The 2.45 nm diameter correlates with the first absorbance peak (510 nm) and can be calculated using equation 1. The emission spectrum was obtained by using a 350 nm excitation wavelength and measuring the fluorescence emission as a function of wavelength. The absorbance peak seen at 510 is blue-shifted to the emission peak at 523 nm. The emission peak seen at 700 nm is the doubling peak caused by the initial excitation wavelength at 350 nm.

Figure 2.4 shows a thermal analysis of the 2.45 nm quantum dots. As the oven temperature increases, the organic material will decompose leaving the inorganic CdSe providing a percent difference by weight (wt-%). This product has a 23% by-weight inorganic content.

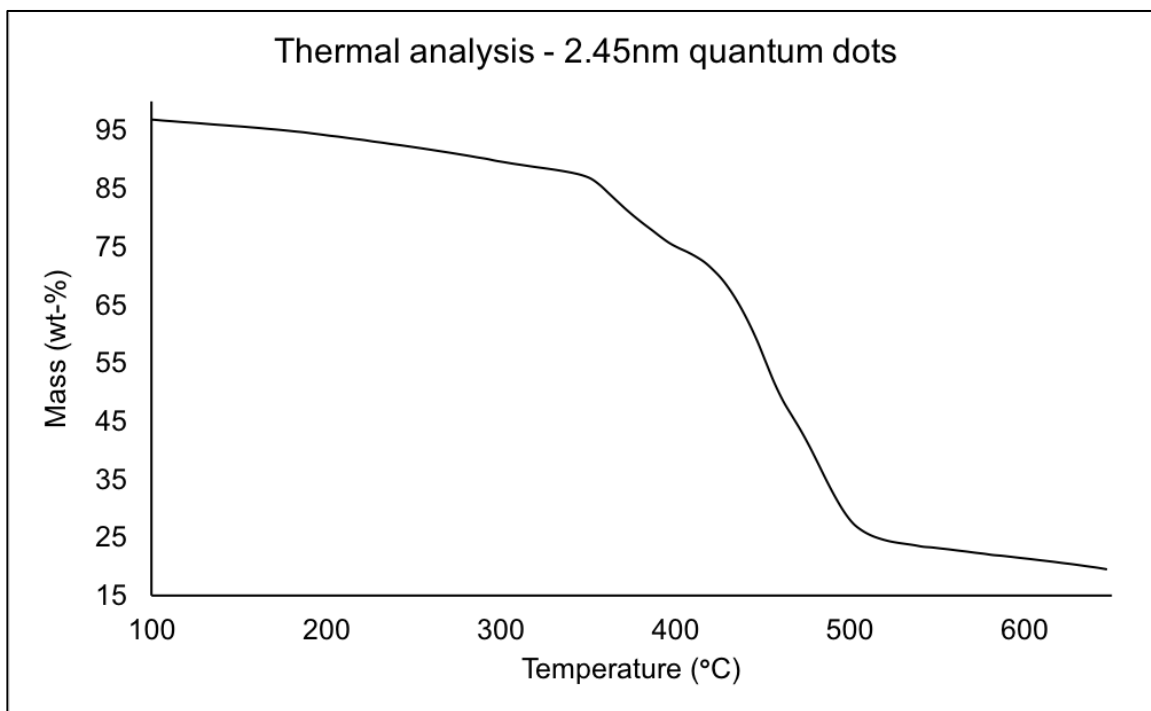


Figure 2.4. Thermal gravimetric analysis (TGA) of 2.45 nm quantum dots.

Figure 2.5 shows a TEM image of the 2.45 nm quantum dots. These quantum dots appear to be roughly spherical which serves as a confirmation that the product formed. Using *imageJ* software and the scalebar provided by the TEM instrument, an average diameter of 1.22 ± 0.2 nm ($n = 100$) was measured with n measuring the total number of particles measured. This deviates significantly from

the average diameter of 2.45 nm calculated from the UV-vis λ_{\max} using the empirical fit of Peng et. al.⁶ CdSe quantum dot diameters obtained using UV-vis λ_{\max} are used throughout this work because the resolution of our TEM is not sufficient to enable accurate sizing of these very small particles.

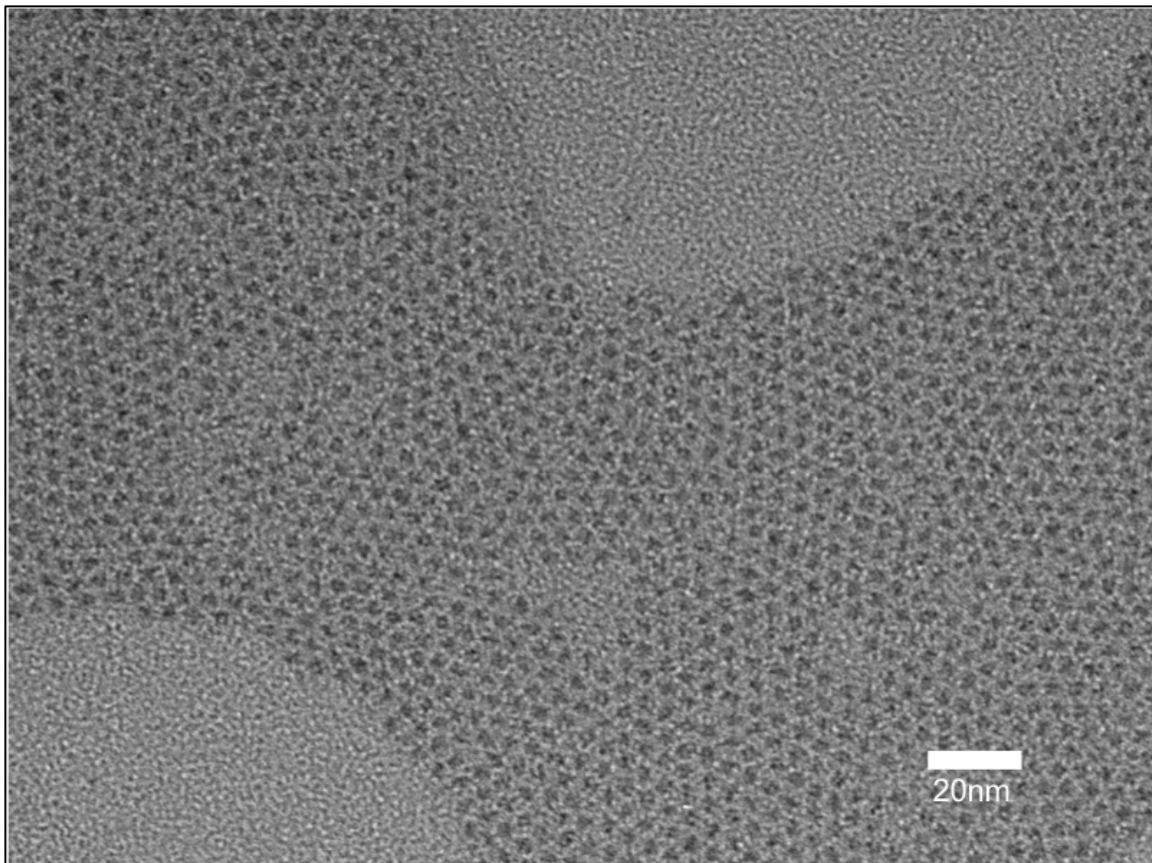


Figure 2.5. TEM of CdSe quantum dots. Average diameter of 1.22 ± 0.2 nm ($n = 100$) was measured. This deviates significantly from the average diameter of 2.45 nm calculated from the UV-vis λ_{\max} using the empirical fit of Peng et. al.⁶

2.2.2.2 CdSe@CdS Nanorods

2.2.2.2.1 Synthesis

This synthesis was adapted from literature.²⁰ CdSe quantum dots (0.67g) (2.2.2.1) and sulfur (0.5g) was added to a clean 20 mL vial. Under argon, TOP (15 mL) was injected and vessel was pressurized. The solution was stirred overnight and stored using an aluminum foil wrap to protect the sample from light.

TOPO (15g), ODPA (1.4g), HPA (0.4g), and CdO (0.4g) was added to a clean 3-neck round-bottom flask and heated to 150°C under vacuum for 30 minutes while stirring at 300 rpm. The flask was then backfilled with argon and heated to 300°C until the mixture became clear. At this point, TOP (9 mL) was injected to the hot solution with stirring at 450 rpm. This was held for 20 minutes. The solution was then heated to 380°C where TOP:S (9 mL) stock solution was quickly injected. The temperature was held at 350°C for 6 minutes after which it is cooled. The minimum reaction temperature as the room temperature stock solution was injected and the time to recover temperature were recorded. Toluene was injected at 110°C after the reaction time had completed.

Purification consisted of three steps with varying amounts of toluene and ethanol. The crude sample was divided between two centrifuge tubes and diluted to a total volume with toluene (27.5, 22.5, and 12.5 mL total volume) and precipitated using ethanol (22.5, 27.5, 37.5 mL). The final product (pellet) was transferred to a 20 mL vial and dispersed in DCM (~5 mL) and dried with a rotovap and then stored using an aluminum foil wrap to protect the sample from light.

2.2.2.2.2 Characterization

Figure 2.6 shows the expected visual appearance of the final nanorod solution. It exhibits a bright orange color with no visual precipitate. If there appears to be a black substance floating in solution, the likely issue was the cadmium oxide. It is important to make sure to use the cadmium oxide purchased from Sigma Aldrich.



Figure 2.6. Image of completed nanorod reaction solution. It appears vivid orange with no precipitate particles floating in solution or settling at the bottom. This image also shows the 3-neck round bottom flask and how each joint is wrapped carefully with Teflon tape to ensure a moisture tight seal.

Figure 2.7 shows the comparison of the absorption and fluorescence spectra for the CdSe@CdS nanorods. The purpose of this test was to provide evidence of seeded growth. Since the fluorescence peak at around 559 nm is red-shifted from the absorption peak at around 549 nm, seeded growth did occur.²¹

TEM was used to get images of the 66 nm CdSe@CdS nanorods. Figure 2.8 shows an image with a lower left insert of the imageJ software used for the particle sizing. These particles showed an average length of 57 ± 5.4 nm ($n = 153$) and a diameter at roughly half the length of the rod equal to 3.6 ± 0.5 nm ($n = 127$).

TGA provided the percent of organic content for the nanorods samples. Figure 2.9 shows the TGA scan yielding a value of 71% for the inorganic content.

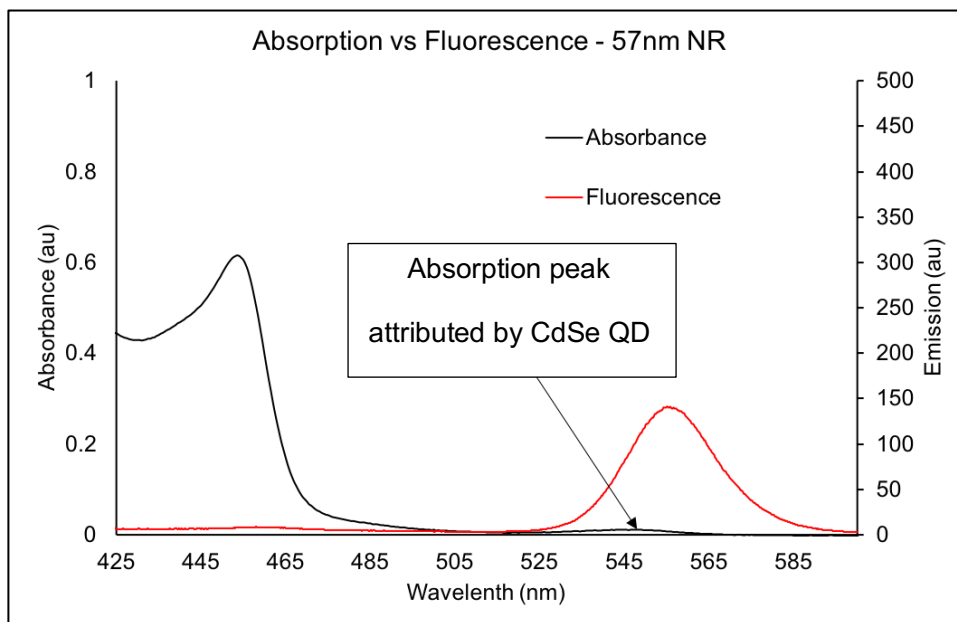


Figure 2.7. Comparison between UV absorption and fluorescence emission of the CdSe@CdS nanorods. There is a small absorption peak seen at 549 nm which is slightly blue-shifted from the fluorescence emission peak at 559 nm.

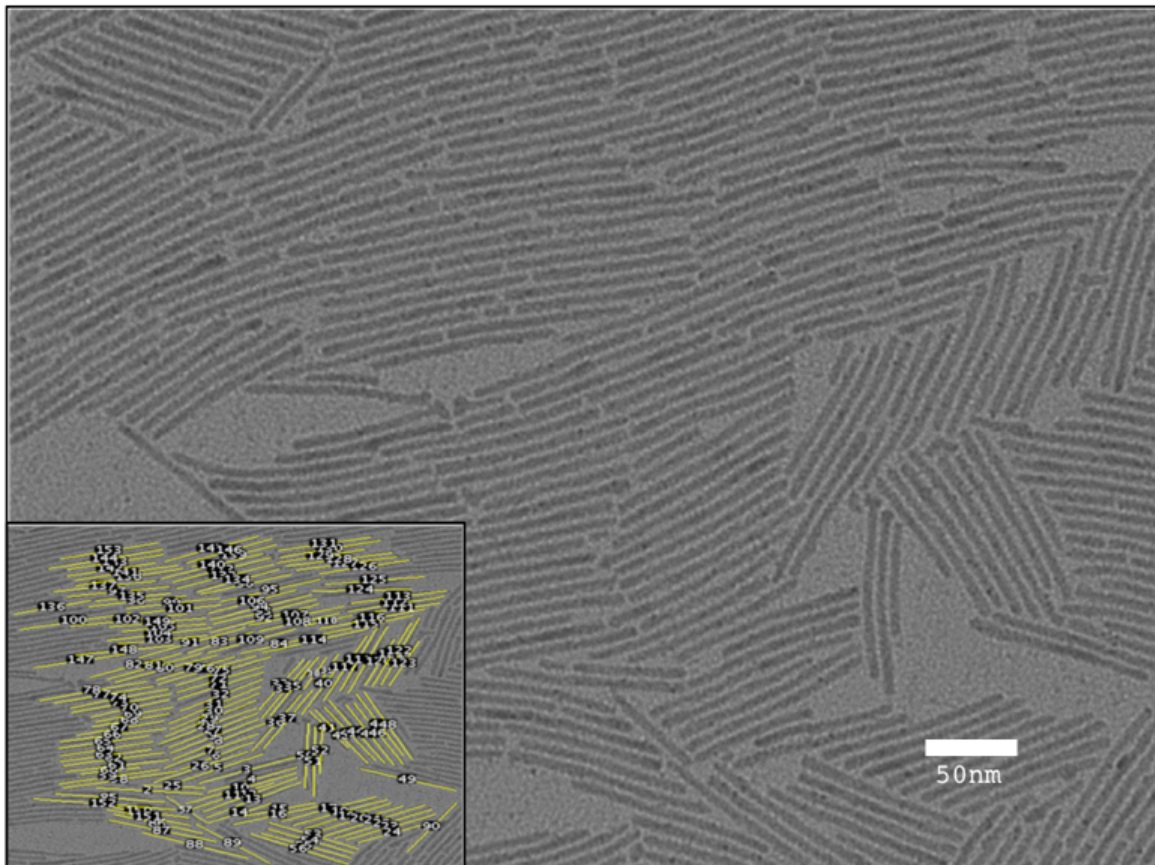


Figure 2.8. TEM of CdSe@CdS nanorods with a length of 57 ± 5.4 nm ($n = 153$) and a diameter of 3.6 ± 0.5 nm ($n = 127$). Length sizing can be seen in the lower left insert.

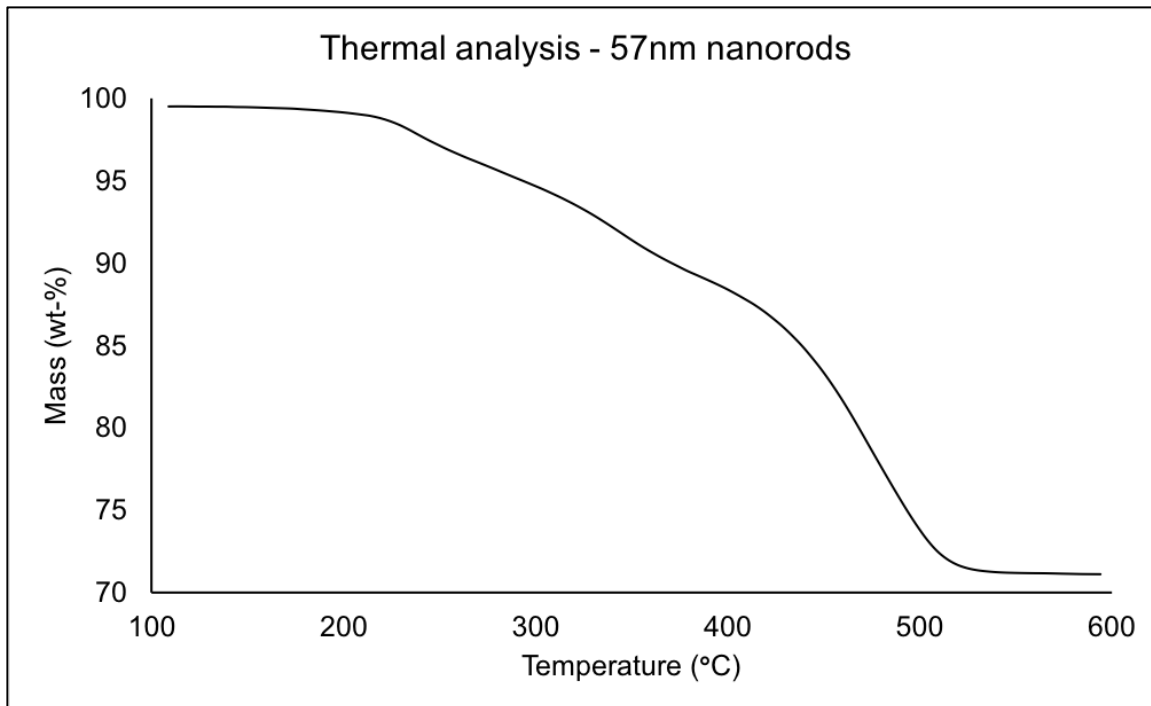


Figure 2.9. Thermal analysis of the 57 nm CdSe@CdS nanorods. This shows the change in weight percentage by mass as a function of increasing temperature. As the temperature increases, the organic content begins to decompose until only the inorganic content remains. This sample showed an inorganic content of 71. %.

2.2.2.3 Thermal deposition: Pt-tipped nanorods

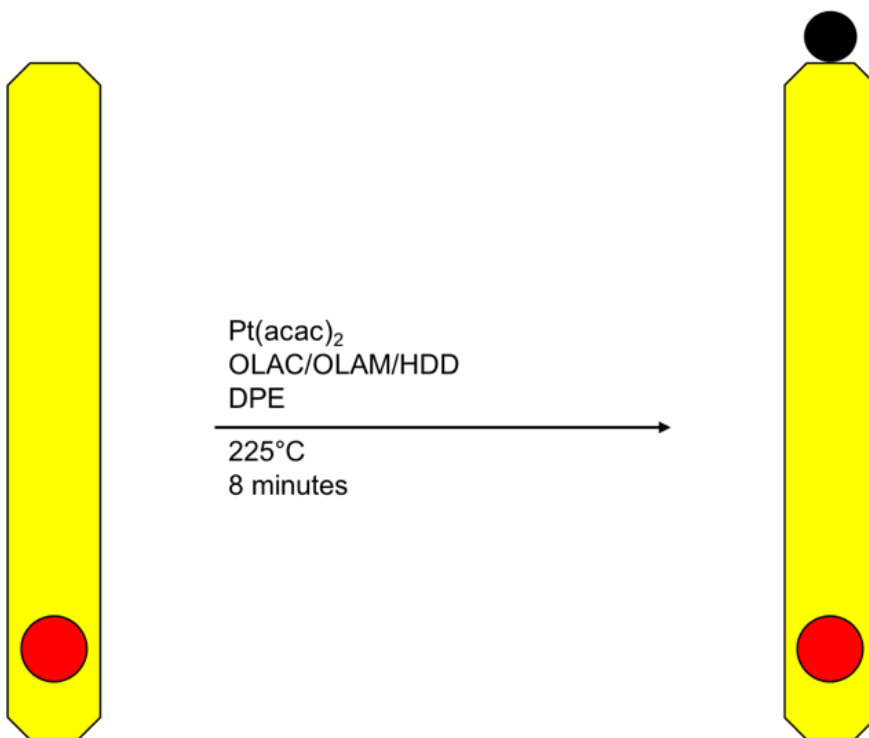
2.2.2.3.1 Synthesis

Scheme 2.1 illustrates the thermal deposition of platinum nanoparticles onto well-defined nanorods as adapted from literature.²²⁻²³ Pt(acac)₂ (25 mg) was used as the platinum precursor, oleic acid (0.2 mL)/oleylamine (0.2 mL) were used as additional supporting ligands, and 1-2-hexadecanediol (0.04 g) was used as a

reducing agent. These reagents were placed into a 50 mL 3-neck round bottom flask along with diphenyl ether (10 mL) as the solvent. CdSe@CdS nanorods (25 mg) and Pt(acac)₂ (25 mg) were dissolved into dichlorobenzene (1.2 mL) in a separate 4 mL vial.

The round bottom was heated to 80°C for 30 minutes under vacuum with stirring at 300 rpm. This was to ensure the reagents were in solution and that all excess water was out of the system. The solution was then heated to 225°C where the 1.2 mL NR/Pt(acac)₂/DCB solution was injected. The reaction took place over 8 minutes after which the solution was taken out of the heating mantle and allowed to cool to around 110°C where toluene (10 mL) was injected to prevent solidification.

Purification consisted of 2 centrifugation steps. The crude product was divided into two 50 mL centrifuge tubes and diluted to 35 mL with toluene. Ethanol (15 mL) was used as a non-solvent to precipitate the particles. Both centrifugation steps were 2500 rpm for 12 minutes both of which showed a green supernatant and orange pellet. The pellets were dispersed and stored in toluene. It's been shown that once the Pt-NR are dried, they become irreversibly aggregated so the nanoparticle suspension in toluene is essential.



Scheme 2.1. Thermal deposition of platinum onto CdSe@CdS nanorods. $\text{Pt}(\text{acac})_2$ is used as the platinum precursor and diphenyl ether (DPE) as the solvent. Oleic acid (OLAC) and oleylamine (OLAM) are used as additional supporting ligands. Hexadecanediol (HDD) is used as the reducing agent to assist in the reduction of the platinum precursor.

2.2.2.3.2 Characterization

Figure 2.10 illustrates a TEM image of Pt-NRs synthesized using thermal deposition using traditional reagents and methods in Scheme 2.1. These are mostly comprised of a “matchstick” configuration which means there is preferential attachment of a single platinum nanoparticle to one end of the nanorod. These rods were synthesized using the 57 nm nanorods which is seen consistent here

and they were measured using *imageJ* to be 56.8 ± 0.6 nm in length and 3.6 ± 0.5 nm in diameter.

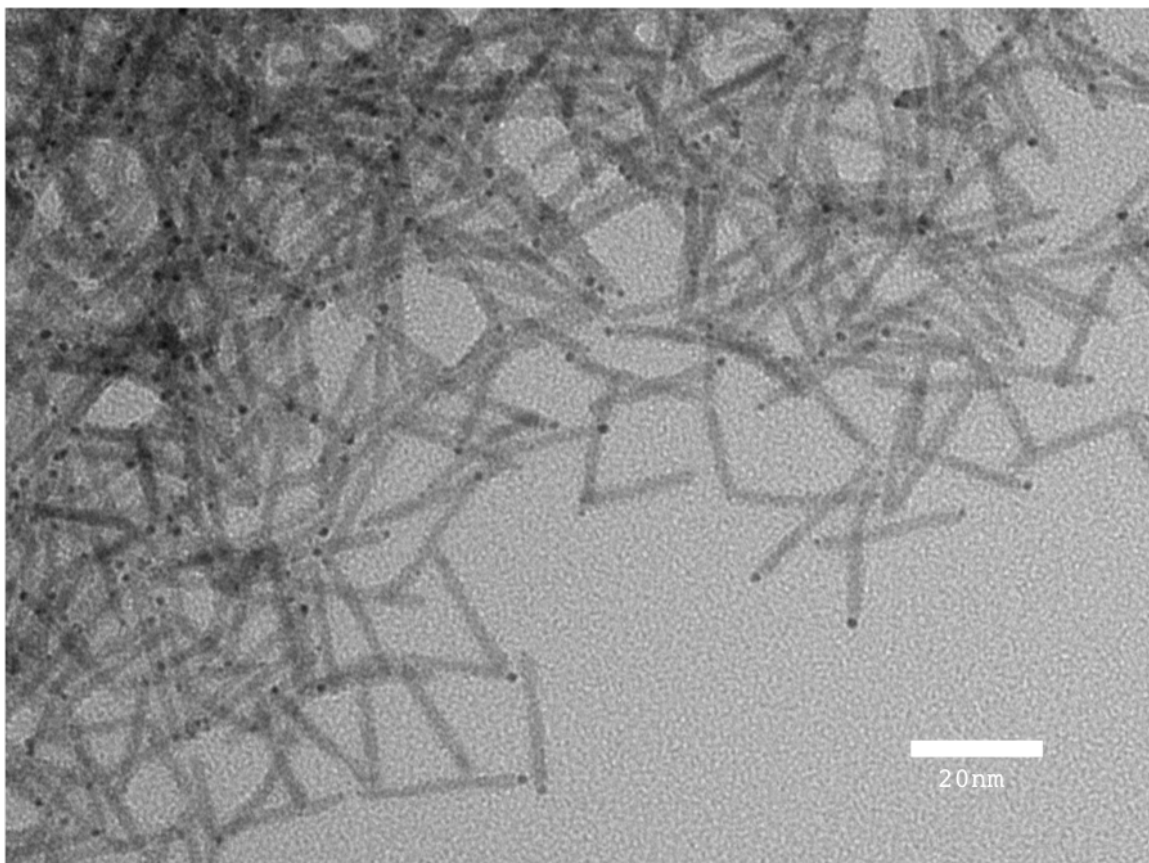


Figure 2.10. TEM of Pt-tipped nanorods synthesized by thermal deposition in diphenyl ether using 57 nm nanorods.

2.2.2.4 [BMIM]Tf₂N

2.2.2.4.1 Synthesis

The synthesis of [BMIM]Tf₂N was adapted from literature.²⁴

Lithium bis(trifluoromethylsulfonyl)imide salt (50g, 0.17mol) and 1-butyl-3-methylimidazolium chloride (30.42g, 0.17mol) were added to a clean 400 mL flask containing DI water (200 mL). The reaction was stirred for 48 hours. There should be a two-phase system observed with the denser [BMIM]Tf₂N forming as the bottom phase.

After 48 hours, the mixture was added to a 1L separatory funnel. The flask was washed with DCM to ensure the product was completely extracted. Multiple smaller washes are preferred to a single large wash. The amount of DCM used in this particular synthesis was around 50 mL but could vary as needed. It was thought that the DCM might add free chloride ions to the [BMIM]Tf₂N, thus giving false positives when the halide content test was completed with the silver nitrate but this was shown to be false. While using purified DCM (washing several times with DI water using another separatory funnel), there were no indication of a difference between the original and the purified and no free halides were detected with either the purified or original DCM using silver nitrate. This shows that it is reasonable to use bulk DCM for this synthesis without fear of free chloride contamination.

After the mixture was added to a separatory funnel, clean DI water (200 mL) was added. The separatory funnel was sealed and shaken vigorously. It is important to relieve the pressure so that the cap doesn't fly off violently or the separatory funnel explodes. The bottom phase was released from the separatory funnel into the original flask. This ensured there was minimal loss in product. The top phase was released into a waste beaker. A small amount of the water phase

(about a milliliter) was placed into a test tube and 2-3 drops of silver nitrate was added. If there was a precipitate that settles to the bottom of the test tube, it indicated free halides present in the wash. Washing was repeated until no precipitate was seen in the wash, and then washing was repeated once more. Typically, it took around 5 washes before the [BMIM]Tf₂N was completely purified of free halides.

The container that the [BMIM]Tf₂N was to be stored in was weighed before adding the new product. This allows one to calculate a percent yield. This reaction should theoretically produce 73.03g [BMIM]Tf₂N but that will vary depending on scale of reaction. For each of the syntheses performed, the yields were: 63%, 88.6%, 95.4%, and 72.6%. I personally performed the purifications for trials two and three while M. Garcia performed purifications for trials 1 and 4.

2.2.2.4.2 Characterization

Figure 2.11 shows the thermal analysis for the lab synthesized [BMIM]Tf₂N. This was to ensure the thermal properties were aligned with those reported in the literature.¹² To compare with figure 6, it complements what is expected from this solvent in regards to the percent weight change as a function of temperature. As this was completed under a nitrogen pure atmosphere, the decomposition is prolonged further than that of the sample in air reported in the literature.

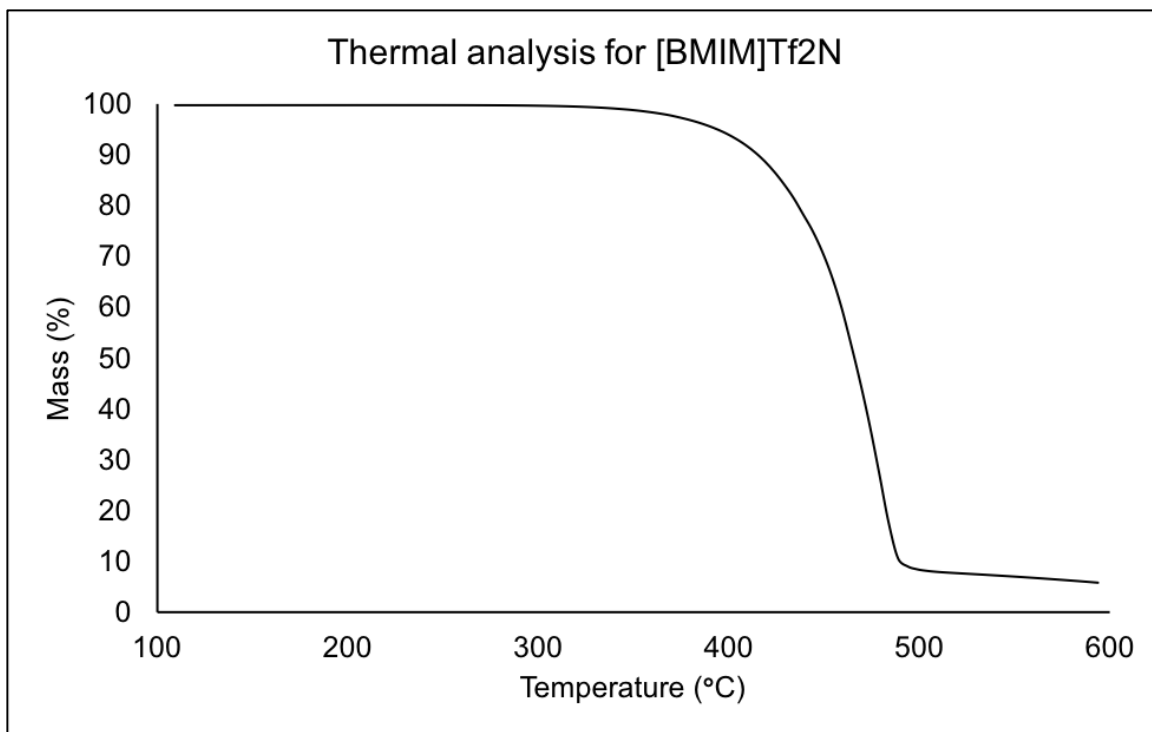
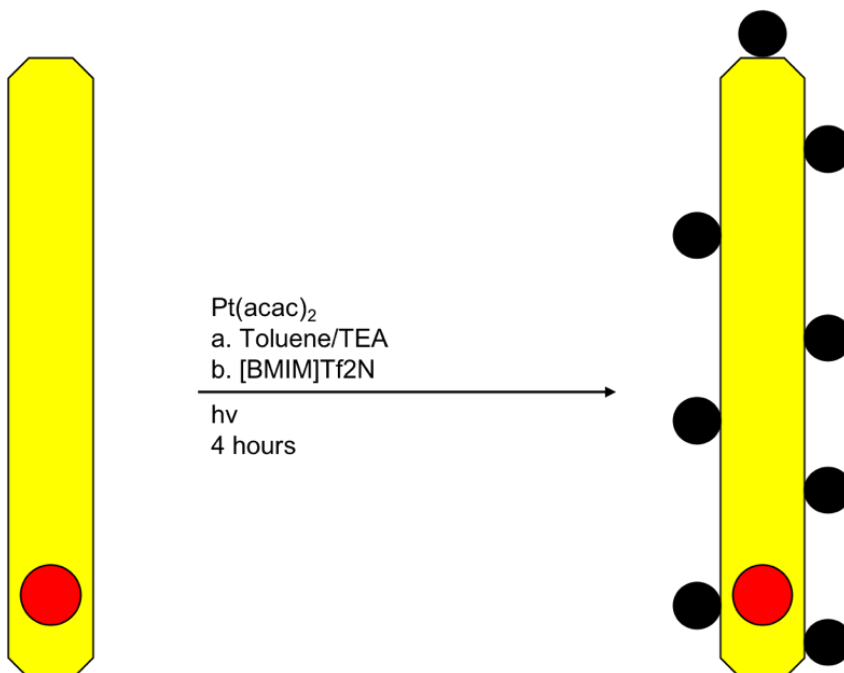


Figure 2.11. Thermal analysis of lab synthesized [BMIM]Tf₂N with heating rate of 10 K min⁻¹ showing the change in weight percent of sample as a function of temperature.

Chapter 3: PLATINUM PHOTODEPOSITION ONTO NANORODS

3.1 Introduction

The synthesis of Pt-tipped nanorods was investigated using a photochemical method adapted from Dukovic and coworkers.²⁵ The photodeposition was performed in two different solvent systems. A toluene system was adapted from literature, and used triethylamine (TEA) as a sacrificial reducing agent.²⁵ [BMIM]Tf₂N was the second solvent system, and acted as the multifunctional solvent, ligand, and reducing agent in the deposition reaction. Scheme 3.1 shows the synthesis of Pt-NR in both (a) toluene/TEA and (b) [BMIM]Tf₂N.



Scheme 3.1. Representation of the photodeposition reaction in either the (a) toluene/TEA system or the (b) ionic liquid system.

3.2 Photodeposition

3.2.1 Toluene/TEA

The photochemical reduction and surface placement of platinum on well defined heterostructures was adapted from literature.²⁵

Toluene (17.2 mL) and TEA (2.8 mL) were added to a 20 mL vial along with Pt(acac)₂ (60 mg) and CdSe@CdS nanorods (20 mg). These reagents were sonicated and added to a 60 mL quartz round-bottom flask with a 1-inch stirbar as seen in figure 3.1. The vessel was fixed directly under a xenon arc lamp and stirred at 400 rpm for 4 hours with the light on. The reaction setup is shown in figure 3.2. After the reaction, the product appeared completely black and seen in figure 3.3.

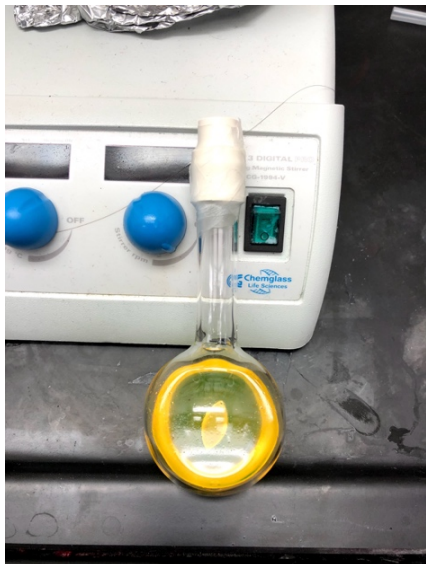


Figure 3.1. Image of the reaction vessel containing the toluene/TEA solvent system for the photodeposition reaction.

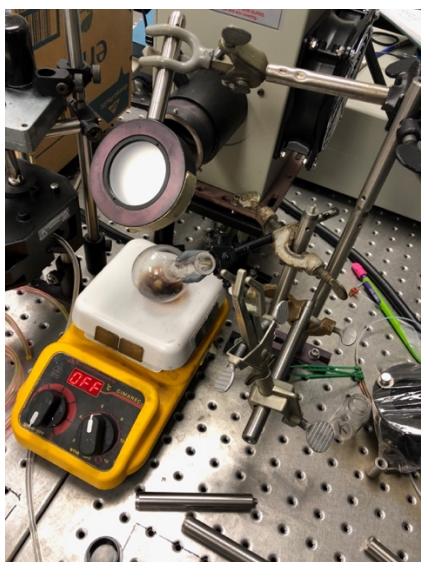


Figure 3.2. Image of the reaction setup for the photodeposition reactions. This setup was used for both of the solvent systems. Note that this was after the reaction was complete as the product is black in color.

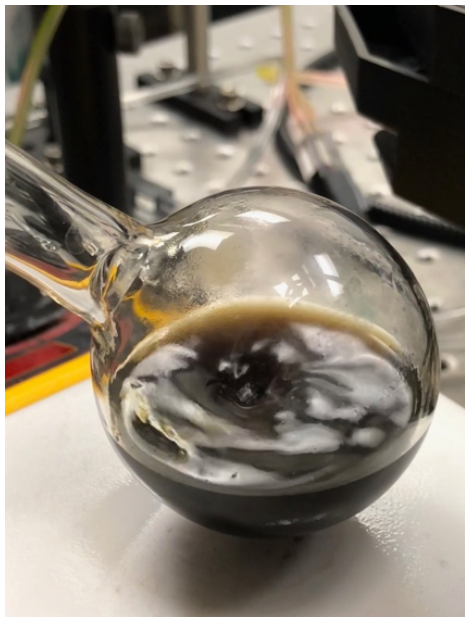


Figure 3.3. Image of the completed reaction solution for the toluene/TEA solvent system.

Purification consisted of two centrifugation steps. The crude product was divided into two centrifuge tubes and diluted to 35 mL using toluene. Ethanol (15 mL) was added as a non-solvent to precipitate the particles. The tubes were spun at 2500 rpm for 12 minutes both times. For the first purification, the pellet appeared black in color with a brown supernatant. For the second purification, the pellet appeared green with a green supernatant. The pellets were dispersed and stored in a total volume of 20 mL in toluene.

3.2.2 [BMIM]Tf₂N

Pt(acac)₂ (60 mg) and CdSe@CdS nanorods (20 mg) were added to about 5 mL of chloroform in a 20 mL vial. Chloroform helps the solids disperse in

[BMIM]Tf₂N. At this point, [BMIM]Tf₂N (3.4 mL) was added to the vial and sonicated. Chloroform was then evaporated using the rotovap. It took about 15 minutes at complete vacuum with the water at around 40°C. The mass of the vial (20.4645g) was compared to the theoretical mass (20.4644g). From this, it was determined that the chloroform was completely evaporated. The remaining [BMIM]Tf₂N was added (16.6 mL) in slow 1 mL increments with shaking in between. These reagents were sonicated and added to a 60 mL quartz round-bottom flask with a 1-inch stirbar, as seen in figure 3.4. The vessel was fixed directly under a xenon arc lamp and stirred at 400 rpm for 4 hours with the light on. After the reaction, the product appeared opaque green/orange in color. Figure 3.5 shows images of the mixture during and after the reaction was complete.



Figure 3.4. Image of the reaction vessel containing the [BMIM]Tf₂N solvent system for the platinum photodeposition reaction.



Figure 3.5. Image of the [BMIM]Tf₂N solvent system photodeposition during (left) and after (right) the reaction.

Purification consisted of a single toluene extraction. The crude product was added to a beaker and toluene was added (10 mL). No shaking or stirring was necessary but 1-2 minutes was required for the extraction to take place as can be seen in figure 3.6. The top layer was the purified Pt-NR sample in toluene. The bottom phase was imaged and consisted of free platinum particles. The top layer was decanted off and purified further using two centrifugation steps. The product was placed into a single centrifuge tube and diluted to 35 mL using toluene. Ethanol was added as a non-solvent to precipitate the particles. Another tube was filled with toluene (35 mL) and ethanol (15 mL) to act as a counter-balance for the centrifuge. The tubes were spun at 2500 rpm for 12 minutes. After each of the

spins, the pellet was a green color and the supernatant was clear. There was a very faint green color for the first supernatant. The hypothesis is that this was product being lost during this step. The pellet was unusually easy to disperse in toluene.

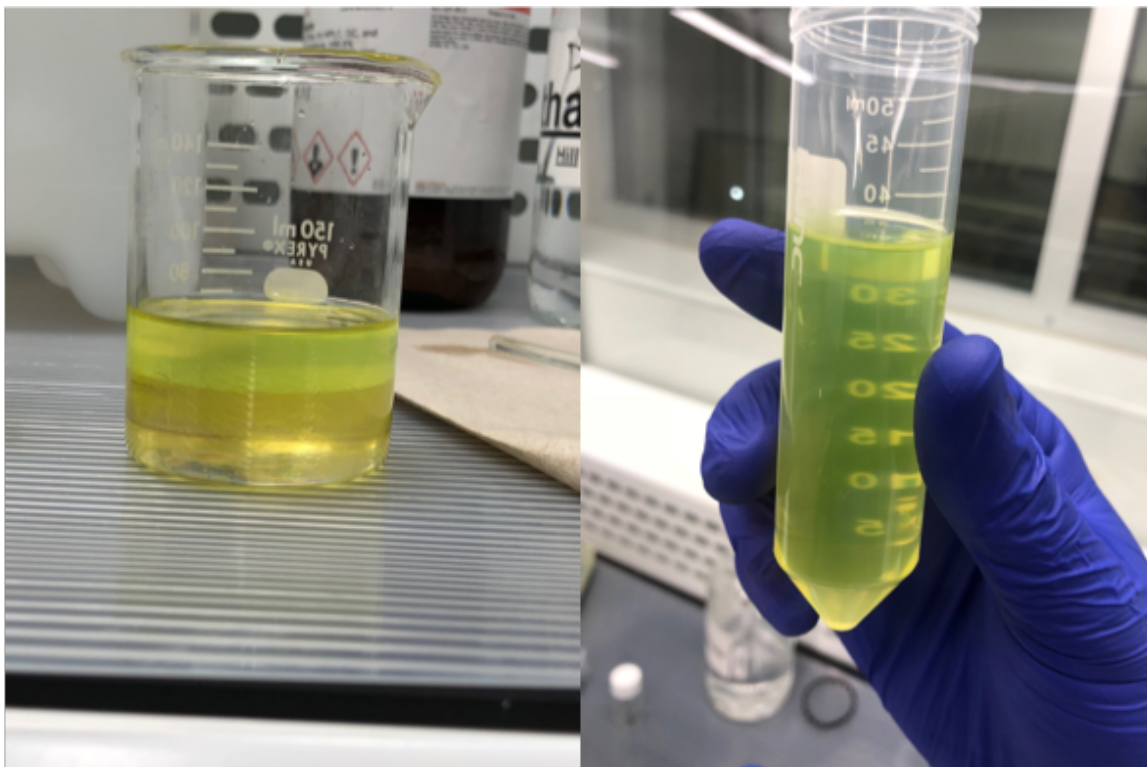


Figure 3.6. Image of the toluene extraction of the platinum photodeposition reaction in the [BMIM]Tf₂N solvent system. Toluene can be seen in the left image extracting out the pure Pt-NR product while leaving the free platinum particles in the bottom layer ([BMIM]Tf₂N). The top layer was extracted and purified more via centrifugation using a 50 mL centrifuge tube (left).

3.3 Characterization

3.3.1 Cadmium concentration

Figure 3.7 shows the concentration results for two separate photodeposition reactions of platinum onto CdSe@CdS nanorods after the purification of the crude products. The results show that the concentration of the toluene/TEA Pt-NR sample was 0.12 mg/mL while the concentration of cadmium in the [BMIM]Tf₂N system was 0.071 mg/mL. These are important because when preparing to compare the performance of these nanorods, the concentrations must be equal to ensure a fair comparison.

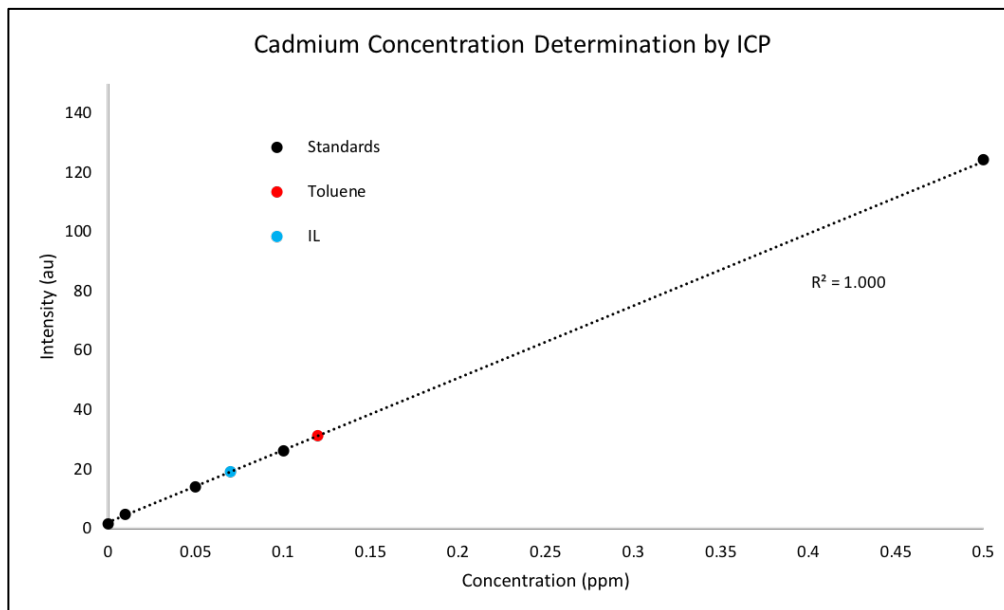


Figure 3.7. Cadmium standard calibration for ICP. Standardized cadmium samples were prepared: 0, 0.01, 0.05, 0.5, 2.5, 0.1, and 0.5 mg/mL and used as calibration for the ICP intensity ratios.

3.3.2 TEM

Figure 3.8 shows a TEM image of the Pt-NRs synthesized in the toluene/TEA solvent system. These rods have an average length of 56.8 ± 0.4 nm ($n = 100$) and a diameter of 3.4 ± 0.2 nm ($n = 100$). Because they were synthesized using the 57 nm nanorods described previously, it is apparent that there was little to no malformations or damage caused to these rods.

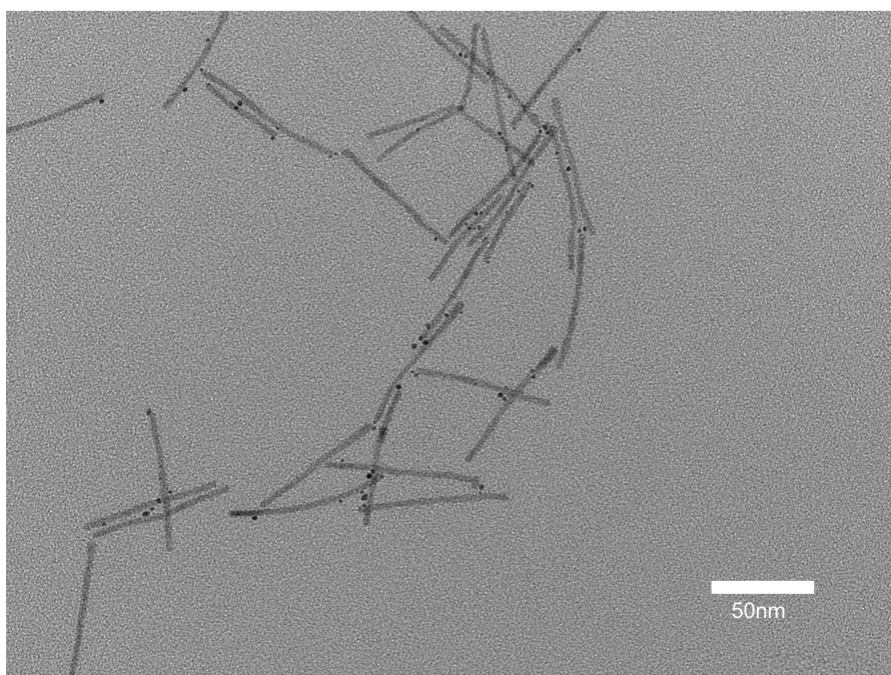


Figure 3.8. Image taken by TEM of Pt-NRs synthesized in the toluene/TEA solvent system. These rods were prepared using 57 nm nanorods. The rods shown here have an average length of 56.8 ± 0.4 nm ($n = 100$) and a diameter of 3.4 ± 0.2 nm ($n = 100$).

Figure 3.9 shows Pt-NRs that were synthesized in the [BMIM]Tf₂N solvent system. These rods were also synthesized using the 57 nm nanorods. They show an average length of 57.1 ± 0.3 nm ($n = 100$) and an average diameter of 3.5 ± 0.2 nm ($n = 100$). This too shows no apparent damage to the rods that can be seen by this instrument.

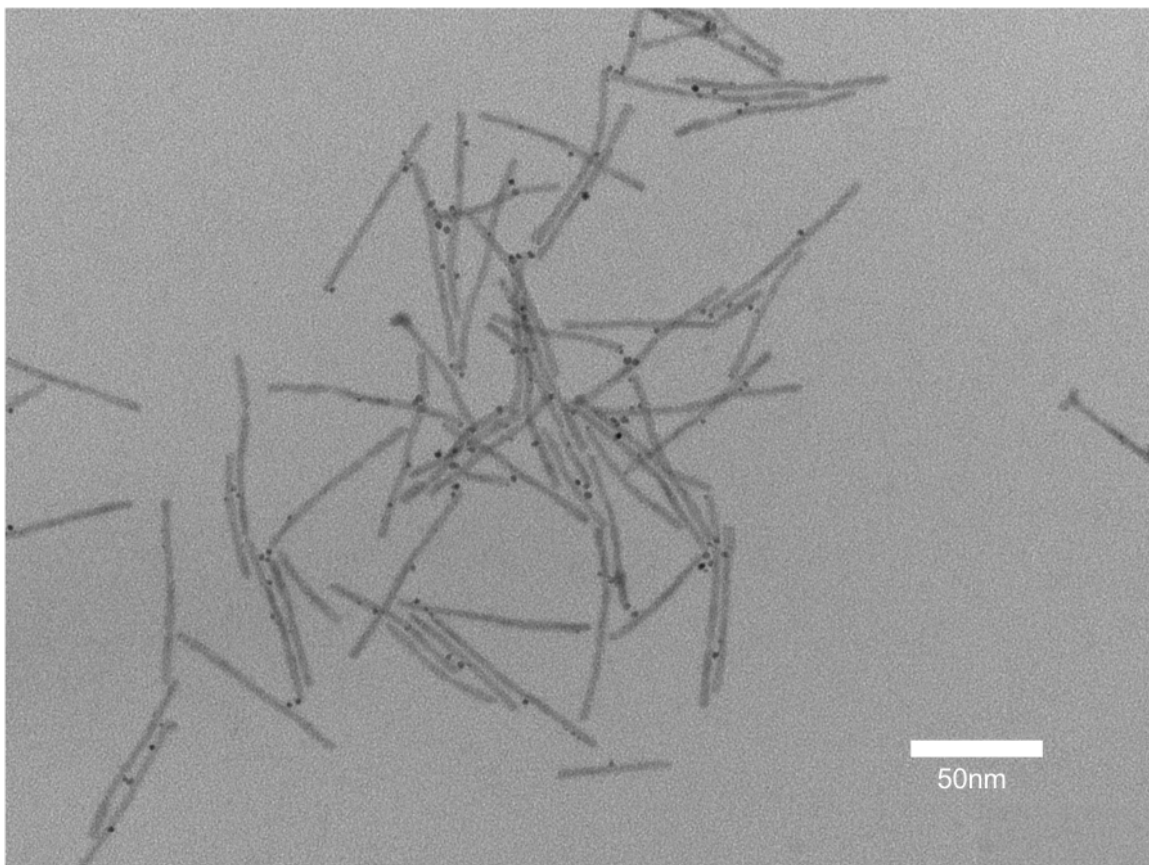


Figure 3.9. Pt-NRs synthesized in the [BMIM]Tf₂N solvent system. These rods had an average length of 57.1 ± 0.3 nm ($n = 100$) and an average diameter of 3.5 ± 0.2 nm ($n = 100$).

3.4 Discussion

These nanorods were synthesized in two different solvent systems. Comparing the images taken by TEM, these rods look very similar. The goal of this research is to test to see if there is a difference in performance based solely upon the synthetic conditions linking performance to synthetic history. Both sample showed nanorods with uncontrolled platinum placement. To support the argument that the platinum was affixed to the rods and not just laying on top in the image, it is important to point out the lack of free platinum anywhere in the image. Because the purifications were conducted using a well-known solvent/non-solvent method, the products were purified consistently and produced a clean sample image with the absence of free platinum. In the case of the [BMIM]Tf₂N solvent system, it is predicted that toluene extraction was sufficient to remove free platinum particles from the product. This conclusion is based on the fact that after the first centrifugation, the supernatant did not appear to have any discoloration other than the faint green tint that was consistent with the color of the product. This is also based on images obtained from the bottom phase of this system that did not contain nanorods, only free platinum.

Chapter 4: PERFORMANCE RESULTS

4.1 Introduction

Methylene blue (MB) is a well-known dye that is used to test the reduction performance of materials. The dye naturally degrades in the presence of light but that degradation can be increased with the addition of a catalyst. The Pt-NRs are a photocatalyst so they are able to speed up the degradation of methylene blue dye. A series of methylene blue experiments were ran to compare the performance of Pt-NRs that were synthesized in the toluene/TEA and [BMIM]Tf₂N systems. To gauge the degradation of methylene blue, UV-Vis spectroscopy was used. There is a prevalent peak seen between 600-700 nm. By monitoring this peak, the decrease in its absorbance will be proportional to the amount of methylene blue remaining in solution.

4.2 Methylene Blue Degradation

Table 4.1 shows the experiments conducted to compare the performance of the differently synthesized yet visually identical Pt-NRs. Two control experiments were conducted to show the natural degradation of methylene blue without the presence of the catalyst. Then, the methylene blue experiment was conducted in the solvent identical to the one in which the Pt-NRs were synthesized. To test if the solvent was a major factor in the degradation of methylene blue, the

degradation experiments were also conducted in the solvent system opposite of the one they were synthesized in.

Platinum-tipped Nanorods	Solvent used in MB Reactions
No Pt-NRs	Toluene
No Pt-NRs	[BMIM]Tf ₂ N
Toluene/TEA	Toluene
[BMIM]Tf ₂ N	[BMIM]Tf ₂ N
Toluene/TEA	[BMIM]Tf ₂ N
[BMIM]Tf ₂ N	Toluene

Table 4.1. Series of methylene blue experiments conducted to test the performance of Pt-NRs that were synthesized in either the toluene/TEA or the [BMIM]Tf₂N system.

4.2.1 Control Experiments

The performance evaluation of platinum-tipped nanorods was adapted from literature.²⁶ The experimental procedure consisted of the addition of 1 mg of methylene blue in either toluene (10 mL) or [BMIM]Tf₂N (10 mL). Sonication was required to fully disperse the dye into toluene. In order to dissolve methylene blue in [BMIM]Tf₂N, the chloroform must be used as described previously (Section 3.2.2). The methylene blue was transferred to a 60 mL quartz round-bottom flask

and placed under a xenon lamp for 2 hours. Kinetic aliquots (0.6 mL) were taken at 15-minute intervals to show the change in absorbance as a function of time (time 0 was taken directly before the lamp was turned on). These aliquots were placed in a 4 mL vial that were wrapped in aluminum foil to protect from light. UV absorption spectra were taken of each of these sample using the methods mentioned previously.

4.2.2 MB degradation in solvent identical to synthesis solvent

For the methylene blue degradation in toluene (9 mL), the experiment consisted of the addition of 1 mg of methylene blue into toluene. Sonication was required to fully disperse the dye. Pt-NRs that were synthesized in the toluene/TEA solvent system were added (1 mL) to the pre-dispersed methylene blue solution. The solution was added to a 60 mL quartz round-bottom flask and placed directly under the xenon lamp. Aliquots and UV spectra were taken identical to the control experiments.

Pt-NRs were synthesized in [BMIM]Tf₂N and had a cadmium concentration of 0.078 mg/mL. They were stored in toluene. To adjust the concentration to be equal to that of the rods synthesized in toluene/TEA, 1.69 mL of the Pt-NR synthesized in IL (stored in toluene) was evaporated under full vacuum and 40°C for 10 minutes until dry. This solid and methylene blue residue (1 mg) was dispersed in chloroform (1 mL). [BMIM]Tf₂N (1.69 mL) was added to the chloroform dispersion and the chloroform was evaporated off using the method mentioned

previously. The Pt-NRs and MB solution in [BMIM]Tf₂N degradation experiment was identical to the control experiment. It was seen that the absorption of methylene blue from time 0 to time 1 (15 minutes) went completely to zero absorbance. The aliquot samples can be seen in figure 4.1. The image on the left shows the general methylene blue degradation experimental setup while the image on the right shows time points 0 and 1 of the initial [BMIM]Tf₂N experiment using the Pt-NRs synthesized in [BMIM]Tf₂N. These results indicated that the reaction proceeded faster than the kinetic time points were able to show. A second experiment was ran taking time points ever minute for 5 minutes. These time points were still not sufficient to clearly depict a trend. A third experiment was performed taking 10 second kinetic samples for 90 seconds. This showed a descending trend of the methylene blue degradation. Figure 4.2 shows these UV spectra and the methylene blue degradation trend.

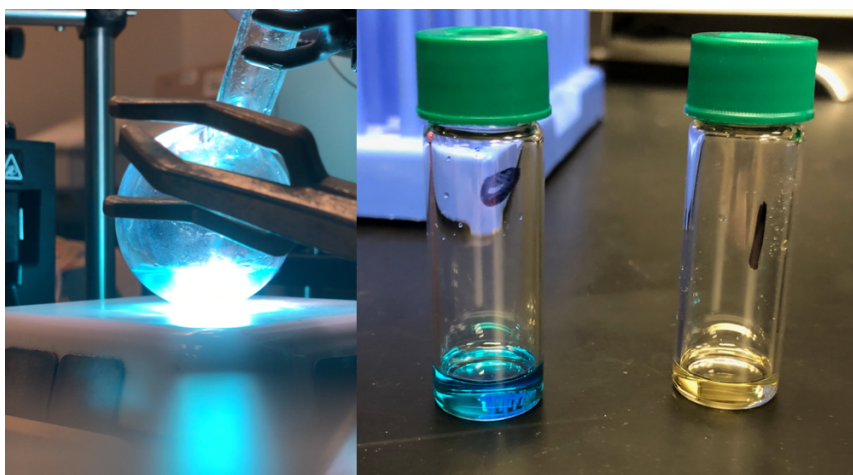


Figure 4.1. Image of the methylene blue degradation setup (left) and the time 0 and time 1 (15-minutes) of the methylene blue degradation experiment in [BMIM]Tf₂N using Pt-NRs synthesized in [BMIM]Tf₂N.

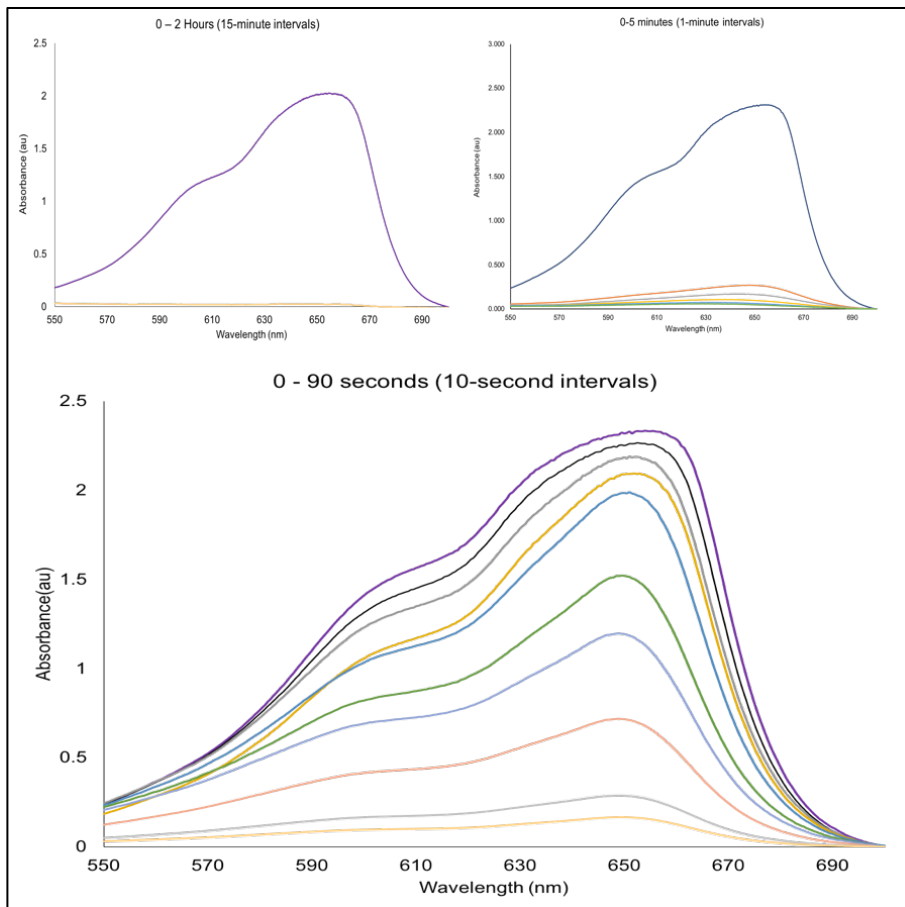


Figure 4.2. UV spectra illustrating the degradation of methylene blue using the Pt-NRs synthesized in the [BMIM]Tf₂N solvent system. Three different degradations were conducted to capture the timeframe of degradation. The initial 0-2 hour experiment with 15-minute kinetic intervals (top-left) and the second experiment (top right) (0-5 minutes, 1-minute intervals) were insufficient. The third experiment (bottom) from 0-90 seconds (10-second intervals) was sufficient to monitor the decrease in absorption as a result of the degradation of methylene blue.

4.2.4 MB Degradation in solvent opposite of synthesis solvent

To test if the solvent was having a major impact of the degradation of methylene blue, two crossover experiments were conducted. A sample containing Pt-NRs synthesized in the toluene/TEA system (1 mL) was dried and dispersed in [BMIM]Tf₂N using methods mentioned previously. Methylene blue (1 mg) was then added using methods previously mentioned.

The Pt-NRs synthesized in [BMIM]Tf₂N were stored in toluene and 1.69 mL of that solution was taken and diluted to 10 mL. Methylene blue (1 mg) was added and sonicated to ensure homogeneity. The degradation experiments were conducted under identical conditions to those of the control experiments.

4.3 Results

Figure 4.3A shows each methylene blue degradation experiment with 15-minute kinetic sample intervals.⁷ The control experiments were consistent, degrading slowly over the two hours ending with a final concentration of methylene blue of 75% (toluene) and 70% ([BMIM]Tf₂N). The degradation conducted in toluene using the Pt-NRs synthesized in toluene/TEA showed an increase in degradation to 60% methylene blue remaining after 30 minutes and ending with a final concentration of about 30% after 2 hours. The Pt-NRs that were synthesized in [BMIM]Tf₂N were so efficient at degrading the methylene blue (in [BMIM]Tf₂N) that 15 minutes was too long to get an accurate representation of the reaction. A second reaction was ran where the first 5 minutes were observed with 1-minute kinetic increments. This result was similar to the initial results with the methylene

blue degrading to about 30 percent in about 1 minute. A third trial was ran to get the first 90 seconds with 10-second intervals. Figure 4.3B shows the combination of the second and third trials of this experiments. The time point from 0-60 seconds are from the third trial while 60-300 seconds were from the second trial. It can be seen from this experiment that the methylene blue in [BMIM]Tf₂N degrades at a much higher rate using the nanorods that were synthesized in [BMIM]Tf₂N.

The crossover experiments were conducted to give an accurate performance comparison of the Pt-NRs. In order to compare these catalysts, they must be in the same solvent system during methylene degradation. This is because the solvent itself will play a role in the absorbance of the dye. Using [BMIM]Tf₂N as the solvent for degradation, the Pt-NRs synthesized in the ionic liquid degraded methylene blue more efficiently between times 0 and 75 minutes than the Pt-NRs synthesized in toluene/TEA, but both experiments ended with a methylene blue concentration of essentially zero. The methylene blue degradation conducted in toluene showed that the Pt-NRs synthesized in the ionic liquid significantly out-performed the Pt-NRs synthesized in toluene/TEA.

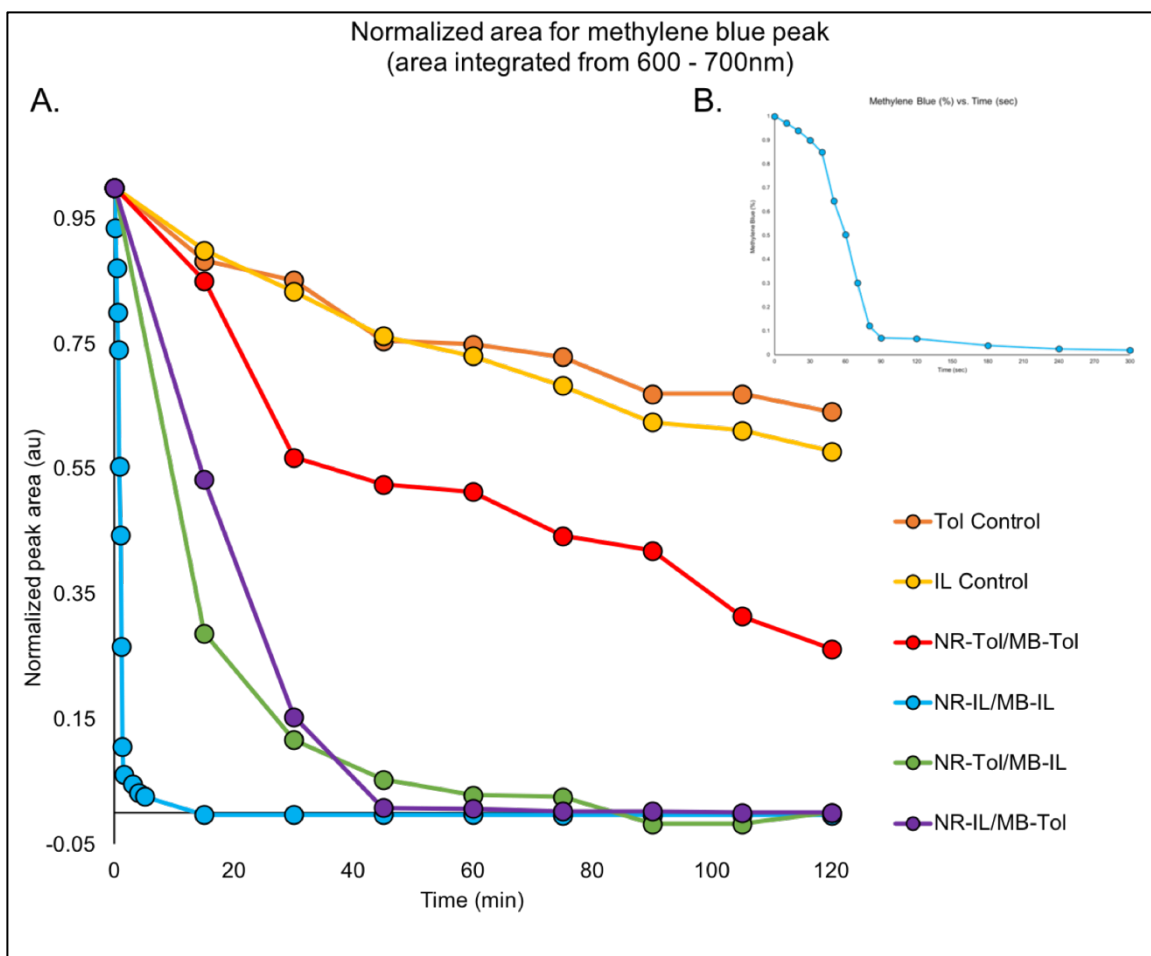


Figure 4.3. Normalized methylene blue degradation experiments in either toluene or [BMIM]Tf₂N and two differently synthesized Pt-NRs (toluene/TEA or [BMIM]Tf₂N) along with control data for both toluene and [BMIM]Tf₂N. **(A)** Normalized peak areas were integrated from the UV-Vis spectra (600-700 nm) for kinetic samples taken every 15 minutes. The time 0 integrated absorbance was normalized to 1 and it was assumed that no MB degradation had taken place before the start of the experiments. **(B)** Minutes 0-5 for the Pt-NRs synthesized in [BMIM]Tf₂N used to degrade methylene blue in [BMIM]Tf₂N.

Chapter 5: CONCLUSIONS

This work has investigated the synthesis and performance of platinum-deposited cadmium sulfide nanorods containing a cadmium selenide core using two different solvent systems, toluene/TEA and [BMIM]Tf₂N. These products were synthesized using a photochemical reaction taking advantage of the well-defined structures of the nanorods. In toluene solution, triethylamine was used as a sacrificial reducing agent to aid in the reduction of the platinum metal; however, in the system containing the ionic liquid, [BMIM]Tf₂N itself acted as the reducing agent. This ionic liquid also acted as a ligating solvent. Because ionic liquids act as a weakly binding ligand, this could possibly explain the increase in the degradation of methylene blue. Compared to the control experiment and degradation experiments conducted in toluene, there is a significant difference in the performance for these nanorods. In fact, every methylene blue degradation that contained Pt-NRs that came into contact with [BMIM]Tf₂N in some way showed better performance than those that did not. It was clear from the control experiment that the IL itself was not causing the increase in degradation as the rate of degradation was very similar to that of the control conducted in toluene.

Surface availability is a main reason for exploration into systems containing nanomaterials. Tightly binding ligands used (TEA) in the synthesis of the platinum nanoparticles will decrease the surface area available to perform catalysis. When an ionic liquid is introduced as the solvent, it can act as a ligand supporting the formation of particles without reducing the surface area. As the ionic liquid is a fluid matrix, never binding permanently to the rod surface, the particles are free to move

about the matrix without ever coming into contact with other particles, thus preventing aggregation while keeping the surface available for catalysis.

These hypotheses will need to be further explored to determine exactly why the Pt-NRs perform better if they come into contact with an ionic liquid. Future work could include the introduction of a different ionic liquid such as [BMIM]BF₄ to test if [BMIM]Tf₂N is the determining factor in this performance increase, or if synthesis with other ionic liquids can show similar performance enhancements. It would also reveal if there was a significant difference in the ionic liquid used in the synthesis of Pt-NRs or the methylene blue degradation experiments.

Another avenue for exploration would be to synthesis quantum dots and nanorods using only ionic liquids. This would have a few advantages over the original syntheses. First, because the ionic liquid can act as the solvent, ligand, and reducing agent, it could possibly allow for the syntheses to be done in tandem meaning that the particles would never have to be removed from the solvent to move to the next synthetic step. This would remove all tightly binding ligands from the reactions and eliminate the possibility of generating additional surface defects. If the performance of those Pt-NRs isn't as high as the one reported here, then that would suggest that the surface defects played a role in the degradation experiments.

Another area that could be explored would be the reusability of ionic liquids, which are already known to be relatively green solvents.²⁷ The performance comparison to the Pt-NRs synthesized in neat IL is still to be explored. This would be an interesting concept and would support the notion that the tandem syntheses

mentioned previously would be a feasible approach. If the results showed a drastic negative effect from the reuse of the ionic liquid, then the syntheses would have to be purified and put into neat IL. Literature suggests that the reused IL performs just as well as the neat IL in different systems but would have to be explored further for this system.²⁷

Functionalization of ionic liquids is yet to be explored in this system and could provide better control over the placement of platinum particles onto the surface of the nanorods. Systems with a single platinum particle per rod shows a dramatic increase in catalytic performance.²⁶ There are possible avenues for exploration into the synthesis of shape-controlled particles using the unique designer and functionalization qualities of ionic liquids to initiate preferential growth using binding of the imidazolium cations to the surface facets of nanoparticles. It has been shown that thiol functionalized ionic liquids have increased the overall control over the synthesis of nanoparticles, so it has the potential to do the same for the growth of nanorods and the deposition of platinum nanoparticles onto their surface. Ionic liquids and their functionalized counter-parts have the potential to dramatically advance the field of nanomaterials and catalytic solar energy production.

Chapter 6: References

1. Alivisatos, A. P., Semiconductor Clusters, Nanocrystals, and Quantum Dots. *Science* **1996**, 271 (5251), 933-937.
2. Valden, M.; Lai, X.; Goodman, D. W., Onset of catalytic activity of gold clusters on titania with the appearance of nonmetallic properties. *Science* **1998**, 281, 1647-50.
3. Bell, A. T., The impact of nanoscience on heterogeneous catalysis. *Science* **2003**, 299 (5613), 1688-91.
4. LaMer, V. K.; Dinegar, R. H., Theory, Production and Mechanism of Formation of Monodispersed Hydrosols. *Journal of the American Chemical Society* **1950**, 72 (11), 4847-4854.
5. Vreeland, E. C.; Watt, J.; Schober, G. B.; Hance, B. G.; Austin, M. J.; Price, A. D.; Fellows, B. D.; Monson, T. C.; Hudak, N. S.; Maldonado-Camargo, L.; Bohorquez, A. C.; Rinaldi, C.; Huber, D. L., Enhanced Nanoparticle Size Control by Extending LaMer's Mechanism. *Chemistry of Materials* **2015**, 27 (17), 6059-6066.
6. Yu, W. W.; Qu, L.; Guo, W.; Peng, X., Experimental Determination of the Extinction Coefficient of CdTe, CdSe, and CdS Nanocrystals. *Chemistry of Materials* **2003**, 15 (14), 2854-2860.
7. Amirav, L.; Alivisatos, A. P., Photocatalytic Hydrogen Production with Tunable Nanorod Heterostructures. *The Journal of Physical Chemistry Letters* **2010**, 1 (7), 1051-1054.

8. Jun, Y. W.; Lee, J. H.; Choi, J. S.; Cheon, J., Symmetry-controlled colloidal nanocrystals: nonhydrolytic chemical synthesis and shape determining parameters. *J Phys Chem B* **2005**, *109* (31), 14795-806.
9. Wegner, S.; Janiak, C., Metal Nanoparticles in Ionic Liquids. *Top Curr Chem (Cham)* **2017**, *375* (4), 65.
10. Antonietti, M.; Kuang, D.; Smarsly, B.; Zhou, Y., Ionic liquids for the convenient synthesis of functional nanoparticles and other inorganic nanostructures. *Angew Chem Int Ed Engl* **2004**, *43* (38), 4988-92.
11. Feng, W.-q.; Lu, Y.-h.; Chen, Y.; Lu, Y.-w.; Yang, T., Thermal stability of imidazolium-based ionic liquids investigated by TG and FTIR techniques. *Journal of Thermal Analysis and Calorimetry* **2016**, *125* (1), 143-154.
12. Kosmulski, M.; Gustafsson, J.; Rosenholm, J. B., Thermal stability of low temperature ionic liquids revisited. *Thermochimica Acta* **2004**, *412* (1-2), 47-53.
13. Maton, C.; De Vos, N.; Stevens, C. V., Ionic liquid thermal stabilities: decomposition mechanisms and analysis tools. *Chem Soc Rev* **2013**, *42* (13), 5963-77.
14. Cao, Y.; Mu, T., Comprehensive Investigation on the Thermal Stability of 66 Ionic Liquids by Thermogravimetric Analysis. *Industrial & Engineering Chemistry Research* **2014**, *53* (20), 8651-8664.
15. Janiak, C., Ionic Liquids for the Synthesis and Stabilization of Metal Nanoparticles. *Zeitschrift für Naturforschung B* **2013**, *68* (10), 1059-1089.

16. Dupont, J.; de Souza, R. F.; Suarez, P. A., Ionic liquid (molten salt) phase organometallic catalysis. *Chem Rev* **2002**, *102* (10), 3667-92.
17. Dupont, J.; Scholten, J. D., On the structural and surface properties of transition-metal nanoparticles in ionic liquids. *Chem Soc Rev* **2010**, *39* (5), 1780-804.
18. Dupont, J.; Fonseca, G. S.; Umpierre, A. P.; Fichtner, P. F. P.; Teixeira, S. R., Transition-Metal Nanoparticles in Imidazolium Ionic Liquids: Recyclable Catalysts for Biphasic Hydrogenation Reactions. *Journal of the American Chemical Society* **2002**, *124* (16), 4228-4229.
19. Peng, X.; Schlamp, M. C.; Kadavanich, A. V.; Alivisatos, A. P., Epitaxial Growth of Highly Luminescent CdSe/CdS Core/Shell Nanocrystals with Photostability and Electronic Accessibility. *Journal of the American Chemical Society* **1997**, *119* (30), 7019-7029.
20. Carbone, L.; Nobile, C.; De Giorgi, M.; Sala, F. D.; Morello, G.; Pompa, P.; Hytch, M.; Snoeck, E.; Fiore, A.; Franchini, I. R.; Nadasan, M.; Silvestre, A. F.; Chiodo, L.; Kudera, S.; Cingolani, R.; Krahne, R.; Manna, L., Synthesis and micrometer-scale assembly of colloidal CdSe/CdS nanorods prepared by a seeded growth approach. *Nano Lett* **2007**, *7* (10), 2942-50.
21. Puzder, A.; Williamson, A. J.; Zaitseva, N.; Galli, G.; Manna, L.; Alivisatos, A. P., The Effect of Organic Ligand Binding on the Growth of CdSe Nanoparticles Probed by Ab Initio Calculations. *Nano Letters* **2004**, *4* (12), 2361-2365.

22. Mokari, T.; Rothenberg, E.; Popov, I.; Costi, R.; Banin, U., Selective growth of metal tips onto semiconductor quantum rods and tetrapods. *Science* **2004**, *304* (5678), 1787-90.
23. Mokari, T.; Sztrum, C. G.; Salant, A.; Rabani, E.; Banin, U., Formation of asymmetric one-sided metal-tipped semiconductor nanocrystal dots and rods. *Nature Materials* **2005**, *4* (11), 855-863.
24. Mudring, A.-V.; Babai, A.; Arenz, S.; Giernoth, R., The “Noncoordinating” Anion Tf₂N⁻ Coordinates to Yb²⁺: A Structurally Characterized Tf₂N⁻ Complex from the Ionic Liquid [mppy⁺][Tf₂N⁻]. *Angewandte Chemie International Edition* **2005**, *44* (34), 5485-5488.
25. Dukovic, G.; Merkle, M. G.; Nelson, J. H.; Hughes, S. M.; Alivisatos, A. P., Photodeposition of Pt on Colloidal CdS and CdSe/CdS Semiconductor Nanostructures. *Advanced Materials* **2008**, *20* (22), 4306-4311.
26. Nakibli, Y.; Kalisman, P.; Amirav, L., Less Is More: The Case of Metal Cocatalysts. *J Phys Chem Lett* **2015**, *6* (12), 2265-8.
27. Wang, Y.; Maksimuk, S.; Shen, R.; Yang, H., Synthesis of iron oxide nanoparticles using a freshly-made or recycled imidazolium-based ionic liquid. *Green Chemistry* **2007**, *9* (10), 1051-1051.